ELSEVIER

XAFS of dinuclear metal sites in proteins and model compounds

Pamela J. Riggs-Gelasco, Timothy L. Stemmler, James E. Penner-Hahn *

Department of Chemistry, University of Michigan, Ann Arbor, MI 48109-1055, USA

Received 22 September 1994; in revised form 10 February 1995

Contents

* Corresponding author.

Abstract

Extensive use has been made of X-ray absorption fine structure (XAFS) spectroscopy for investigating the local structural environment of metal ions in metalloproteins. Although it is widely accepted that XAFS provides accurate structural information for the nearest neighbors to the metal (i.e., the ligands), the use of XAFS for determining metal–metal distances in multi-nuclear proteins is more problematic. We review the origin of the information in XAFS spectra and discuss some of the limitations that apply in extracting structural data from XAFS spectra. Recent advances in the theory and application of XAFS for determining metal–metal distances are reviewed, with particular emphasis on dinuclear iron and manganese proteins and models. For distances less than 3 Å, it is straightforward to determine accurate metal–metal separations using XAFS. For distances > 3 Å, the unique assignment of an XAFS feature to a metal–metal interaction continues to be difficult, despite recent advances in XAFS theory and analysis. However, when additional information is available to constrain the possible metal site structures, XAFS can provide very accurate metal–metal distances. Future developments that may improve this situation are discussed.

Keywords: X-ray absorption fine structure spectroscopy; Multi-nuclear proteins; Metal–metal distances

1. Introduction

X-ray absorption fine structure (XAFS) spectroscopy refers to the structured absorption near an X-ray absorption edge [1]. From analysis of the XAFS oscillations, it is possible, at least in principle, to obtain information about the immediate environment of the X-ray absorbing atom. One of the key attractions of XAFS is that it depends only on the local structural environment of the absorber and does not require the presence of long-range order. This means that XAFS can be used to obtain structural information for non-crystalline samples, and has led to an explosion of interest in the applications of XAFS to metalloproteins. There are numerous excellent reviews both of XAFS in general and of the biological applications of XAFS [2–6].

Briefly, XAFS arises from scattering of the X-ray excited photoelectron by the neighboring atoms. Although in rare cases it is possible to observe scattering from atoms as far as ca. 10 Å from the absorber, disorder typically limits metalloprotein XAFS to much shorter distances ($R_{max} \leqslant 4$–5 Å). It is widely accepted that XAFS can be used to determine the number and type of nearest neighbors and the average bond length from the absorber to the nearest neighbors. Typical accuracies are ± 1

for coordination number and ± 0.02 Å for bond length, while scatterers can be identified to the nearest row of the periodic table. This information has been extremely useful for characterizing the ligation of metal ions in proteins.

In principle, it should be possible to extend this analysis to include next nearest neighbors and thus to determine metal–metal distances in metalloproteins. In practice, this extension has proven problematic owing to the fact that there are almost always carbon atoms at nearly the same distance from the absorber as the metal–metal distance of interest. Thus, it is necessary not only to show that there is a scatterer at ca. 3 Å, but also to show that this scatterer is a metal, not a carbon. The metal–carbon (M···C) and metal–metal (M···M) XAFS signals are readily distinguishable in simple single-shell simulations; thus identifying the origin of a 3 Å feature would appear to be straightforward. However, the question is seldom as simple as telling whether an XAFS feature is from M···C or M···M. A more realistic situation is that in which the XAFS contributions from one or more M···C shells interfere, possibly destructively, with the XAFS from an M···M shell. Under such conditions, unique identification of the M···M scattering can become difficult or impossible. Scott and Eidsness reviewed this situation in 1988 and came to the conclusion that "identification of M···M scattering at $\geqslant 3$ Å in metallobiomolecules is fraught with difficulties and ambiguity" [7]. In particular, they reported observations of both false positives (apparent XAFS detection of M···M scattering from mononuclear complexes) and false negatives (apparent absence of M···M scattering from compounds having crystallographically characterized M···M distances of 3–3.5 Å).

In the last 7 years, there have been several further reports of the use of XAFS to identify M···M distances in proteins and model compounds. Accompanying these, there have been a variety of advances in XAFS theory, in data analysis, and in experimental methods which can potentially improve the prospects for identifying M···M distances. In particular, the available XAFS scattering functions, including both single and multiple scattering, are significantly improved. Scott and Eidsness suggested that "better scattering functions or treatment of multiple-scattering effects" might improve the detectability of M···M XAFS [7]. The present review explores the extent to which this has occurred, i.e., the extent to which XAFS can now be used to obtain reliable metal–metal distances in metalloproteins.

As in the earlier study [7], we have not considered sulfur bridged clusters such as those found in the ferredoxins. In such cases, detection of M···M XAFS is usually reliable, both because of the relative rigidity of M_2S_2 units, which leads to strong M···M XAFS, and because of the weakness of outer shell M···C scattering from cysteine ligands, which leads to decreased interference. Rather, we have focused primarily on oxo-, carboxylato-bridged dinuclear clusters, since this structure occurs frequently and since this is a challenging test for identifying M···M XAFS.

2. XAFS background

As noted above, the structural information in XAFS arises from scattering of the X-ray excited photoelectron by the atoms (scatterers) surrounding the absorbing

atom. A general expression for the XAFS is given in Eq. 1,

$$\chi(k) = \sum_{s} \frac{N_s A_s(k) S_0^2}{k R_{as}^2} \exp\left(-2R_{as}/\lambda(k)\right) \exp\left(-2k^2\sigma_{as}^2\right) \cdot \sin\left(2kR_{as} + \phi_{as}(k)\right) \qquad (1)$$

where $\chi(k)$ is the fractional modulation in the absorption coefficient above the edge, $k = \sqrt{2m(E-E_o)/\hbar^2}$ is the photoelectron wavevector, N_s is the number of scatterers at a distance R_{as}, $A_s(k)$ is the backscattering amplitude, S_0^2 is an inelastic loss term, $\lambda(k)$ is the photoelectron mean-free path, σ^2 is the mean-square deviation in R_{as}, ϕ_{as} is the phase-shift that the photoelectron wave undergoes in passing through the potentials of the absorbing and scattering atoms, and the sum is taken over all shells of scatterers. The amplitude term in Eq. 1 contains factors (e.g., S_0^2, $\lambda(k)$) that are necessary for calculating the XAFS ab initio, but that do not contain information that is directly relevant to determining the metal site structure. In practice, Eq. 1 is usually simplified along the lines of Eq. 2. In Eq. 2, S is a scale factor which may, in some implementations, be treated as k-dependent. Many of the recent developments in XAFS revolve around the assumptions and approximations that are used to obtain the effective amplitude functions, $A_s'(k)$.

$$\chi(k) = \sum_{s} \frac{N_s A_s'(k) S}{k R_{as}^2} \exp\left(-2k^2\sigma_{as}^2\right) \cdot \sin\left(2kR_{as} + \phi_{as}(k)\right) \qquad (2)$$

There are several ways in which Eqs. 1 and 2 may contain the information necessary to characterize a dinuclear site. Most obviously, $\chi(k)$ may contain a component that can be unambiguously attributed to M⋯M XAFS. This can be used to demonstrate that a dinuclear site exists. More often, it is known from other measurements that a dinuclear site exists, but the identity of the bridging ligand(s) is unknown. If XAFS can be used to determine the M⋯M distance, this can sometimes be used to deduce the bridging ligation. Finally, there are cases where XAFS can be used to identify a particular ligand directly. For example, short M–O distances can be characteristic of bridging oxo ligands and thus can be used to define the dinuclear site structure.

3. Recent developments in XAFS

3.1. XAFS amplitude and phase parameters

Inherent in Eqs. 1 and 2 is the assumption that the backscattering amplitude depends only on the identity of the scatterer. This derives from the so-called plane-wave approximation, in which the curvature in the photoelectron wave is ignored and the photoelectron is treated as a plane wave. For energies well above the X-ray edge (high k, short photoelectron wavelength) or for long absorber–scatterer distances this is a fairly reasonable assumption. It is not, however, a good assumption for most of the useful XAFS region. This is particularly true for protein data, where signal-to-noise concerns often limit the accessible k range.

The two initial approaches to XAFS analysis were to determine empirical ampli-

tude and phase functions utilizing model compounds of known structure [2,3] or to use the ab initio XAFS parameters calculated by Teo and Lee [8,9]. Both approaches make use of the plane-wave approximation. In the case of empirical amplitude and phase functions, the assumption that amplitude and phase are transferable from the model to the unknown will only be true if the chemical environments, particularly the bond lengths, are identical in the model and the unknown. If there is a change in bond length, the scattering functions will change. The widely utilized Teo–Lee parameters were based on the plane-wave approximation and thus they are not strictly valid for any real system. However, by appropriate calibration and by limiting analysis to higher k data $(k \geqslant 4 \text{ Å}^{-1})$, the Teo–Lee parameters were found to give very accurate bond lengths and reasonable coordination numbers for simple structures [2,10].

Despite their success, it is now widely recognized that the Teo–Lee parameters give a fairly poor description of the XAFS, and in particular do not do a good job of reproducing the XAFS amplitude at low k. Similar problems can arise for empirical amplitude and phase parameters if the model compounds are not chosen very carefully. Amplitude errors, especially at low k, can have a profound influence on the detectability of protein M$\cdots$M scattering. This is because M$\cdots$M interactions are often characterized by fairly large disorder parameters (σ^2). The information necessary to identify a M$\cdots$M interaction may be a weak signal that is present only at low k. Small errors in describing the amplitude of the majority component can severely distort the appearance of the minority M$\cdots$M signal.

Recently, several solutions to the plane-wave approximation have been developed. The simplest is a set of ab initio amplitude and phase parameters calculated by McKale et al. [11–13]. These utilize a curved-wave rather than a plane-wave approximation to give tables of $A_s(k,R)$ and $\phi_{as}(k,R)$. With appropriate calibration, these allow extension of XAFS analyses to somewhat lower k. The McKale parameters have been widely utilized and, again, give quite accurate bond lengths and reasonable coordination numbers, at least for first shell analyses. However, recent careful comparisons between theory and experiment have shown that the McKale parameters also have significant errors at low k [14]. The best approach to XAFS amplitude and phase calculations to date are the programs FEFF, developed by Rehr and co-workers [15–17], and EXCURVE92, developed by Gurman, Binsted and co-workers [18,19]. These programs appear to give essentially equivalent results and have allowed extension of XAFS analyses to much lower k (k_{min} ca. 1.5 Å^{-1}). It should be noted, however, that the earlier versions of EXCURVE (through EXCURVE90) utilized a different potential function for calculating the atomic structure and consequently gave significantly poorer results, particularly at low k [14].

3.2. Multiple scattering

In addition to the development of curved-wave XAFS calculations, a second important advance in XAFS theory has been the development of accurate treatments of multiple scattering phenomena. Multiple-scattering refers to the fact that the X-ray excited photoelectron can be scattered by two (or more) atoms prior to returning to

the absorbing atom. Eqs. 1 and 2 assume that only single-scattering is important. This is always a good assumption for first shell XAFS, and is often a reasonable assumption at high k. However, at low k (i.e., low photoelectron energy), multiple scattering can be important. Multiple scattering is particularly strong if the two scattering atoms are nearly collinear. In this case, the XAFS due to the multiple scattering pathway (absorber→scatterer 1→scatterer 2→scatterer 1→absorber) can be as much as an order of magnitude stronger than that due to the single scattering pathway (absorber→scatterer 2→absorber) [20–22]. Failure to account for multiple scattering can lead to serious errors in both XAFS amplitude and phase, with consequent errors in the apparent coordination number and bond length.

Multiple scattering is extremely angle dependent. For scattering angles less than ca. 150° (the angle A–S_1–S_2 in the example above), multiple scattering is quite weak and can often be ignored. However, for angles between 150° and 180°, multiple scattering must be considered. The angle dependence of multiple scattering means that XAFS can, at least in principle, provide direct information about bond angles. Although there are several examples of multiple scattering calculations being used to reproduce observed XAFS structure, there are very few examples in which multiple scattering has actually been used to extract unique angular information from an XAFS spectrum. This failure is related to the relatively limited information content of an XAFS spectrum (see below).

In biological systems, multiple scattering is most important for ligands such as CO, NO, and CN^-, as well as for the outer shell carbon and nitrogen atoms in histidine imidazoles (see Fig. 1). For dinuclear systems where the bridging atom is nearly collinear with the metals, multiple scattering can significantly enhance the detectability of the M$\cdots$M XAFS. This geometry is, however, uncommon in biological systems. The principal importance of multiple scattering for M$\cdots$M XAFS is that failure to correctly account for multiple scattering can interfere with the analysis of the M$\cdots$M signal. In particular, typical M$\cdots$M distances are often in the range 3–4 Å, which is a region in which imidazole multiple scattering can be important [20].

The EXCURVE programs were the first to provide a convenient approach to multiple scattering. More recently, multiple scattering versions of FEFF have been introduced [22] and other approaches are under development [23]. With the availability of these programs, it is now possible to perform fairly accurate calculations of the multiple scattering contributions that are expected for a particular geometric structure and thus it has become possible to make use of multiple scattering in XAFS analysis.

3.3. XAFS data analysis

In addition to improvements in XAFS theory, there have also been several recent advances in XAFS data analysis. In principle, XAFS analysis involves a straightforward application of non-linear least-squares fitting using Eq. 1. Problems can arise, however, when the available XAFS data do not contain sufficient information to answer certain structural questions. In recent years there has been a growing recogni-
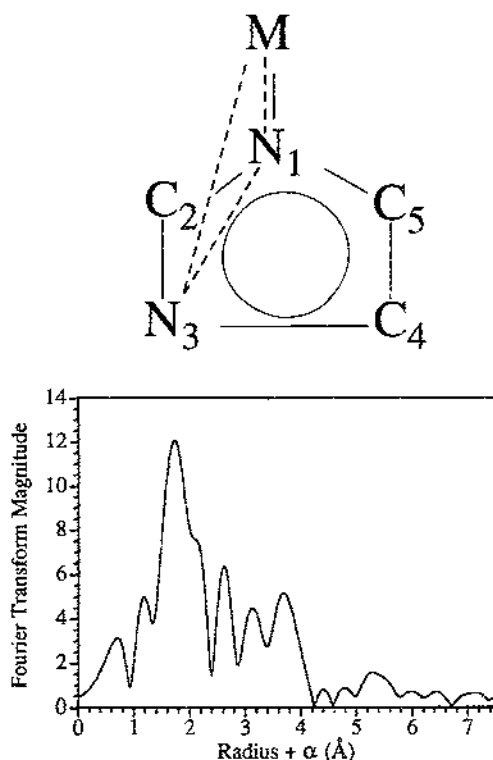
Fig. 1. Top: Schematic illustration showing one of the dominant multiple scattering pathways for imidazole (dashed line). Bottom: Fourier transform of the XAFS spectra for $Mn(imidazole)_6Cl_2$ calculated for $k = 1.5–11.5$ Å^{-1} using k^3 weighted data. Theoretical calculations (FEFF) suggest that the first two FT peaks (1.8 and 2.5 Å) arise from $M–N_1$ and $M·(C_2/C_5)$ single scattering. The outer two peaks (3.2 and 3.8 Å) are due to interference between $M–(N_3/C_4)$ single and multiple scattering contributions.

tion of the limitations of XAFS and of the importance of carefully controlling the number of variable parameters that are refined in least-squares analyses.

3.4. Fourier filtering

It is common in XAFS analysis to isolate the contributions from a single shell using Fourier filtering. The Fourier transform of an XAFS spectrum gives a pseudo radial distribution function of electron density around the absorbing atom [3]. Fourier filtering refers to the procedure in which a single peak within this frequency distribution is back Fourier-transformed into k space.

Ideally, Fourier filtering greatly simplifies the curve fitting problem, since then only a single shell of scatterers needs to be considered (this amounts to dropping the summation in Eqs. 1 and 2). The danger of Fourier filtering is that low symmetry metal sites, such as those often found in metalloproteins, do not necessarily give rise to well resolved shells of scatterers. The potential hazards of Fourier filtering are

illustrated in Fig. 2. The upper plot shows the Fourier transform of the simulated XAFS signal for three oxygen scatterers at 1.9 Å and three oxygen scatterers at 2.1 Å. The magnitude of the Fourier transform in the upper figure appears to show nearly baseline resolution between the two shells. Given these data, it would be tempting to use Fourier filtering to isolate the XAFS into a low-R contribution $(R+\alpha \leqslant 1.6 \text{ Å})$ and a high-R contribution $(R+\alpha \geqslant 1.6 \text{ Å})$. Unfortunately, the apparent resolution is illusory. The lower part of Fig. 2 shows the Fourier transforms of the two individual components. It is clear that, in fact, there is substantial overlap between the two shells. Nearly half of the intensity due to the 2.1 Å shell appears at $R+\alpha \leqslant 1.6 \text{ Å}$. Note also that the peak positions for the combined data (ca. 1.44 and 1.79 Å) are shifted significantly relative to the peaks due to the individual components (ca. 1.51 and 1.71 Å).

Depending on the details of the chemistry of the system, it might be reasonable to assign the low R peak in Fig. 2 to an M–O shell and the high R peak to an M–S shell. The increase in apparent distance for the "second shell" peak makes this seem more reasonable than would otherwise be the case. As discussed above, M–O and M–S XAFS amplitudes are significantly different, thus one would hope that examination of the filtered XAFS would immediately reveal the erroneous M–S assignment. However, due to the leakage of 1.9 Å XAFS into the high R peak and the consequent destructive interference between the 1.9 and 2.1 Å M–O shells, the "second shell" peak does not really look oxygen-like. The filtered "second shell" XAFS is compared with the authentic 2.1 Å M–O spectrum in Fig. 3 (top). It is apparent that there are substantial differences in both the phase and the frequency of the filtered XAFS relative to the true 2.1 Å M–O XAFS. Of greatest concern, however, is the fact that the amplitude for the filtered data now maximizes at $k \approx 8 \text{ Å}^{-1}$ rather than the low k maximum that is expected for M–O XAFS. The amplitude envelope for the filtered data is typical of those seen for higher Z scatterers. To illustrate this point, the lower plot in Fig. 3 shows the best fit that can be obtained if the filtered "second shell"
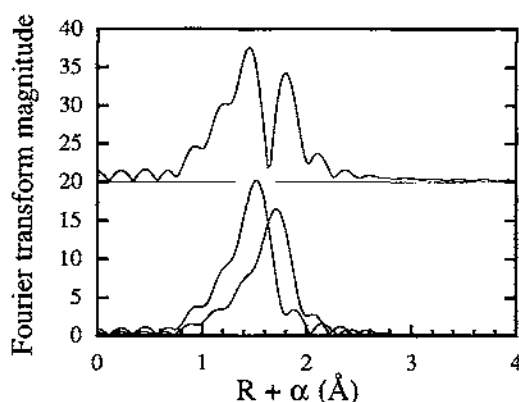

Fig. 2. Fourier transforms of simulated spectra for two shells of M–O with $R = 1.9$ and 2.1 Å. Top: FT of sum of 1.9+2.1 Å shells. Bottom: FTs of 1.9 and 2.1 Å shells calculated individually. All simulations done using FEFF 6.01 with Mn as the central metal. Fourier transforms calculated over $k = 1.5$–15 Å^{-1}.
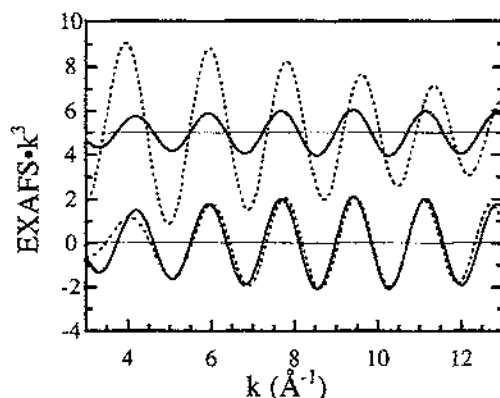
Fig. 3. Fourier filters for data from Fig. 2. Top: Comparison of filtered "second shell" XAFS (solid line) with authentic XAFS of the M–O shell at 2.1 Å. Note differences in phase, frequency, and amplitude due to interference from 1.9 Å shell. Bottom: Best fit (dashed line) of the filtered "second shell" data using a single shell of M–S.

XAFS data are fit using M–S amplitude and phase functions. The resulting parameters are 0.8 S at 2.25 Å with $\sigma^2 = 1 \times 10^{-3}$ Å^2. It is clear that an excellent fit can be obtained and that Fourier filtering has thus succeeded in making a 2.1 Å M–O shell look like a 2.25 Å M–S shell.

This is a contrived example, in so far as there is no evidence that an error of this sort has occurred in any published XAFS. It is nevertheless instructive. We have made no special effort to concoct a situation in which XAFS filtering gives erroneous results. Rather, we have simply used chemically reasonable bond lengths and common analysis procedures to illustrate possible errors. The important lesson is that Fourier filtering can lead to refined structural parameters that are perfectly reasonable but unrelated to the true structure. In order to obtain the fit in Fig. 3, it was necessary to shift E_0 by 14 eV. This provides a clue that something is wrong with the analysis since, in general, E_0 should change by at most a few eV. However, there are numerous examples in the XAFS literature where E_0 is allowed to vary by ± 20 eV, so this is not an unrealistic model.

In the context of identifying M$\cdots$M XAFS, the most likely situation is that a "M$\cdots$M" peak may contain substantial contributions from M$\cdots$C XAFS, even though the M$\cdots$M peak appears to be well isolated in the Fourier transform. Failure to recognize the presence of M$\cdots$C contributions during the curve fitting can alter substantially the apparent M$\cdots$M distance. A more serious problem is that the presence of a new peak in the Fourier transform (for example, a third peak, in addition to the two outer shell peaks expected for histidine imidazole ligands) might reasonably be attributed to M$\cdots$M XAFS. However, as shown in Fig. 2, a new peak can arise solely as the result of interference between two closely spaced shells of scatterers. Attempts to fit the filtered peak can potentially result in erroneous conclusions, as illustrated in Fig. 3. It is clear that Fourier filtering must be used with great caution.

3.5. Number of independent parameters in XAFS

A frequent problem in XAFS analyses is to demonstrate that the inclusion of an additional shell (i.e., an additional sum in Eq. 1) is justified. If perfect data were available, it would be necessary only to determine whether the fit was better or worse when the additional shell was added. In practice, only limited data are available and these data always include some noise contributions. Noise is especially serious for protein XAFS due to the low concentrations that are available. Addition of a new shell often gives a better fit simply as a result of the increase in the number of variable parameters. The solution to this problem is to replace the standard XAFS goodness of fit criterion,

$$F = \sqrt{\sum_{i=1}^{N} (\chi_{obs}(k_i) - \chi_{calc}(k_i))^2 / N} \tag{3}$$

with a statistic that is weighted by the number of free variables. The statistic that has been recommended by the International Committee on Standards and Criteria in XAFS [24] is

$$\epsilon^2 = \frac{(N_{idp}/\nu) \cdot \sum_{i=1}^{N} (\chi_{obs}(k_i) - \chi_{calc}(k_i))^2 / \sigma_i^2}{N} \tag{4}$$

In Eq. 4, ν is the number of degrees of freedom, calculated as $\nu = N_{idp} - N_{var}$ where N_{idp} is the number of independent data points and N_{var} is the number of variables that are refined. The sum is calculated over all of the measured data points, N, and the error at each point is weighted by $1/\sigma_i^2$, where σ_i is the rms uncertainty in χ_{obs}. The $1/\nu$ weighting introduces a penalty for adding additional, unjustified, shells of scatterers.

Application of Eq. 4 is difficult in practice, due to the difficulty in estimating σ_i. As a replacement, several groups have made use of a statistic something like

$$F' = F^2/\nu \tag{5}$$

Eq. 5 retains the $1/\nu$ weighting, but omits the $1/\sigma_i^2$ normalization. It is thus not possible to assign a meaning to the absolute value of F', but it is possible to use F' to tell whether an additional shell has made a fit better or worse.

Precise calculation of the N_{idp} is a matter of some controversy. Initial reports by the International Committee on Standards and Criteria in XAFS [24] suggested

$$N_{idp} = \frac{2\Delta k \Delta R}{\pi} \tag{6}$$

More recently, Stern [25] has suggested that

$$N_{idp} = \frac{2\Delta k \Delta R}{\pi} + 2 \tag{7}$$

is a better estimate of N_{idp}. For the present purposes, the differences between Eqs. 6 and 7 are not important. What is significant is that N_{idp} is a fairly small number. For protein data, k_{max} is typically 13-14 Å^{-1}. By using carefully calibrated curved-wave calculations, it is possible to extend k_{min} to ca. 1.5 Å^{-1}, although much of the published protein XAFS is limited to $k_{min} \approx 3$-4 Å^{-1}. The R range over which XAFS signals are seen depends on the details of the sample, although the best case is typically 1-4 Å. These values give $N_{idp} \approx 20$-25 in the best case, with smaller values being common.

In particular, the R range for filtered data is often much smaller, with $\Delta R \leqslant 0.8$ Å not uncommon. For filtered data it is thus possible to have $N_{idp} \approx 6$. In such cases, it may be impossible to obtain meaningful fits using two shells of scatterers. If three parameters (R, σ^2, and ΔE_o) are refined per shell, then for two shells there are no free parameters. Although the fit may reproduce perfectly the observed data, it is not clear that all, or even most, of the refined structural parameters will be physically meaningful.

One can increase N_{idp} by increasing the filter width or by avoiding filtering altogether. This does not necessarily solve the refinement problem, however, since with the larger R range comes an increase in the number of scatterers that have to be included in order to correctly describe the data. Of particular concern is the fact that the number of degrees of freedom increases linearly with R while the number of scattering atoms increases approximately as R^2 and the number of possible scattering paths, including multiple scattering, increases even more rapidly. This phenomenon makes it unlikely that XAFS alone will ever be able to provide reliable structural information for atoms beyond the third, or perhaps the fourth coordination shell [26].

3.6. Resolution in XAFS

It is frequently the case that biological metal sites contain two or more chemically distinct types of scatterers within a single XAFS "shell". For example, crystallographically characterized dinuclear iron sites often have Fe–O_{oxo} distances of ca. 1.8 Å, Fe–$O_{carboxylate}$ distances of ca. 2.0 Å and Fe–$N_{histidine}$ distances of ca. 2.15 Å within their first coordination shell. Ideally, one would like to be able to determine each of these distances independently. In practice, however, XAFS spectra have severely limited resolution. The achievable resolution can be given [27] as

$$\Delta R \geqslant \pi/2\Delta k \tag{8}$$

which gives $\Delta R \geqslant 0.13$ Å for data to $k_{max} = 12$ Å^{-1}. Eq. (8) means that shells separated by less than ΔR will not be resolvable by XAFS, while shells with a greater separation will, at least in principle, be resolvable. The origin of Eq. (8) is illustrated in Fig. 4. The top trace shows the simulated XAFS oscillations for a pair of scatterers separated by 0.25 Å ($R_1 = 1.75$, $R_2 = 2.00$ Å). There is an obvious beat in the XAFS amplitude at $k \approx 8$ Å^{-1} and it is clear that two shells of scatterers will be required to reproduce the oscillations. A single shell simulation at the average distance (1.875 Å) is out of phase for $k > 8$ Å^{-1} and would obviously not be adequate as a
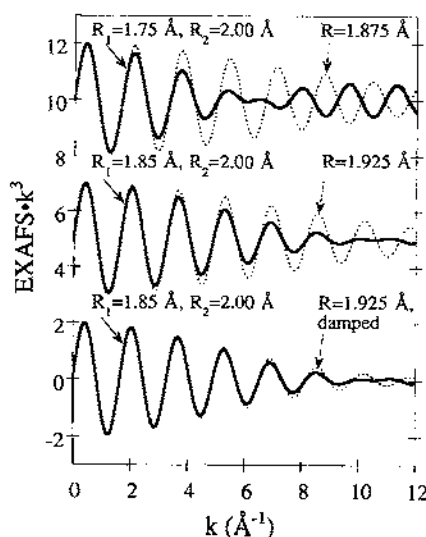
Fig. 4. Simulated XAFS spectra illustrating the effect of resolution on the observed XAFS spectrum. Solid lines are the simulated XAFS for two shells of scatterers separated by 0.25 (top) or 0.15 Å (middle and bottom). Dashed lines are simulated XAFS for a single shell having twice the number of scatterers at the corresponding average distance (1.875 Å, top; 1.925 Å, middle and bottom). In the bottom simulation, the single shell simulation has been damped using a Debye -Waller factor of 5×10^{-3} Å^2.

model for the two-shell XAFS. The middle simulation shows that there is still a beat in the amplitude when ΔR decreases to 0.15 Å ($R_1 = 1.75$, $R_2 = 2.00$ Å) although the beat has moved close to k_{max}. It is nevertheless straightforward to distinguish between the two shell simulation ($\Delta R = 0.15$ Å) and a single shell simulation at the average distance (1.925 Å), as shown by the middle traces. However, if the single shell simulation is damped with an exponential damping factor, it is clear (lower traces) that the single shell simulation now does an excellent job of reproducing the two-shell XAFS oscillations over most of the available range. The damping factor used in this case corresponds to a quite reasonable Debye–Waller factor (see Eqs. 1 and 2) of $\sigma^2 = 5 \times 10^{-3}$ Å^2. It is only at high k, where the noise in an experimental XAFS spectrum is the largest, that the one- and two-shell simulations are distinguishable. Since the differences between the one- and two-shell simulations are smaller than the noise typically seen in protein XAFS spectra, it is unlikely that it would be possible with real data to tell whether this XAFS spectrum represented one or two shells of scatterers, even though $\Delta R > \pi/2\Delta k$. Eq. (8) should thus be regarded as a best case estimate of the achievable resolution, while the real resolution is likely to be substantially worse. A model independent approach to describing disorder in a sample, which avoids the question of how many shells are present, is to describe the XAFS in terms of cummulants [27b]. It is also worth noting that the threshold energy, E_o, is often treated as an adjustable parameter, sometimes with a different E_o being refined for each shell of scatterers. The resolution limits in Eq. 8 assume that there is no ambiguity in E_o. Changes in E_o will affect the location of the beat node and may thus further limit the achievable resolution.

One final point is to note that all of the discussion of resolution has assumed that only a single scatterer type contributes to the XAFS. However, if there are different types of scatterers (e.g., M–O + M–S or M···C + M···M), then additional factors, including phase and amplitude differences, can be used to improve the resolution.

3.7. Effects of limited k range in biological XAFS

In addition to limiting both the amount of information that is available (i.e., N_{idp}) and the available resolution, the limited k range that is accessible in protein XAFS can have profound consequences for structure interpretation. An illustration of this problem is provided by the recent study by Blackburn et al. of a mixed valence Cu dimer [28]. The dimer (see Fig. 5) contains a Cu···Cu bond with a crystallographically characterized Cu···Cu separation of ca. 2.4 Å. The biological relevance of this complex is that it has EPR and XAFS properties similar to those found for the Cu_A sites in N_2O reductase and cytochrome oxidase. Blackburn and co-workers found that the XAFS data for the dimer and for the Cu_A domain of cytochrome oxidase could both be fit using a ca. 2.4 Å Cu···Cu distance. The latter result was surprising in so far as four previous XAFS studies of Cu_A sites did not report a detectable Cu···Cu signal [29–32]. Three of these reports suggested the presence of an unusually long Cu–(S/Cl) feature at ca. 2.6 Å [29–31]. With the latest report, it now appears likely that the "Cu–(S/Cl)" feature described in the earlier studies was actually a Cu···Cu signal.

In view of the frequent claims that XAFS can identify scatterers to within the nearest row of the periodic table, this apparent mis-assignment is both surprising and somewhat alarming. With the benefit of hindsight, it is possible to understand how this happened. Blackburn et al. show that while the Cu···Cu signal is required to fit the XAFS to $k = 16$ Å^{-1}, Cu···Cu and Cu–S do an equally good job of fitting the data when the k range is restricted to $k \leqslant 13$ Å^{-1} (see Fig. 5) [28]. It is only for the data with 13 Å$^{-1} \leqslant k \leqslant 16$ Å^{-1} that Cu and S scatterers can be distinguished.

This illustrates both the importance of measuring XAFS data over as wide a k range as possible and also the necessity of having available good model compounds. Prior to the crystallographic characterization of a mixed valence Cu dimer with a Cu···Cu distance of 2.4 Å, Cu–S scattering appeared to be the chemically most reasonable interpretation of the outer peak in the Cu_A XAFS. With, again, the benefit of hindsight, the refined Debye–Waller factors for the ≈ 2.6 Å Cu–S shell seem questionable. However, they appeared at the time to be less unrealistic than a 2.4 Å Cu···Cu distance.

Given this series of pessimistic observations, it might appear unlikely that XAFS could ever be used to obtain reliable M···M XAFS. The fact is, however, that there are several examples in which XAFS analyses have given accurate M···M distances. Many of these are model studies, where it can be argued that the XAFS outcome was biased by prior knowledge of the crystal structure. However, there are also examples where XAFS predictions have subsequently been shown crystallographically to be correct. In the following, we review a selection of these cases with particular emphasis on attempting to understand the reasons that XAFS has succeeded and those conditions that have led to its failure.
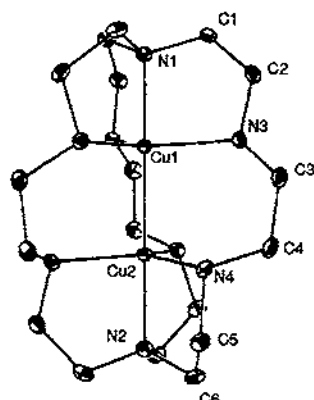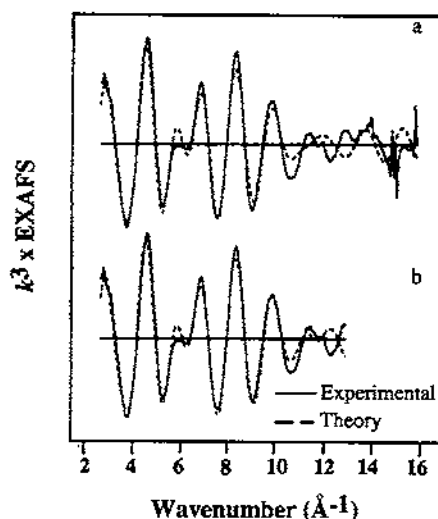
Fig. 5. Mixed valence Cu dimer that may serve as a model for N_2O reductase. Dimer (bottom) has a Cu–Cu bond length of 2.4 Å. When XAFS spectra are fit over the range typical of protein data ($k = 2$–$13 Å^{-1}$), the data can be fit using a Cu–S shell instead of a Cu···Cu shell (fit b). Only when the fit is extended to ca. $16 Å^{-1}$ (fit a) are the errors in the Cu–S fit apparent. The fit using the correct Cu···Cu signal is not shown. Redrawn with permission from Ref. [28].

4. Iron XAFS

4.1. Model studies

There have been numerous XAFS studies of crystallographically characterized dinuclear Fe model complexes. Typically, these have been undertaken as part of a study of dinuclear metalloproteins. In some cases, the model complexes have been used to define metal-scatterer phase and amplitude functions and to define the effects of various structural features on the XAFS oscillations. Two questions are of special

significance for structural determination of dinuclear complexes: (1) is it possible to detect metal–metal interactions at distances > 3 Å in the presence of the inevitable low Z ligands at similar distances?; and (2) is it possible to distinguish bridging motifs (i.e., M(μ-O)M vs. M(μ-OH)M) from analysis of first shell XAFS? In this section, we review the extent to which model studies have been able to answer these questions. The ligation environments of the model compounds that are discussed are shown schematically in Fig. 6.

4.1.1. Detectability of Fe···Fe scattering

The effect of Fe···C scattering on the accurate determination of Fe···Fe distances in dinuclear iron complexes is well documented. The compounds $(HBpz_3Fe)_2O(OAc)_2$, **A** [33], and $(HBpz_3Fe)_2OH(OAc)_2ClO_4$, **B** [34], have been used by several groups as models for the XAFS oscillations seen in dinuclear Fe proteins ($HBpz_3$ = tris(pyrazolyl)borate ion). Kauzlarich et al. [35] found that failure to include a carbon shell at 3.29 Å caused the apparent Fe···Fe distance in **A** to refine to 3.09 Å. When the carbon shell was included, the Fe···Fe distance refined to the crystallographically correct distance of 3.15 Å. Similarly, Hedman et al. [36] found that a reasonable fit for the second shell of scatterers in **A** was only obtained when carbon scattering was included. In addition, however, they found that carbon-only fits gave minima that were indistinguishable from iron-only fits. In particular, if the data range was restricted to $4-12$ Å^{-1} (this is similar to the range used for most metalloprotein XAFS studies), it was extremely difficult to distinguish Fe···Fe from Fe···C backscattering. Finally, Scarrow et al. [37] also analyzed XAFS data for **A**. As in the other studies, they used both Fe and C to model the outer shell XAFS. However, they found that excluding the carbon shell did not significantly alter the refined Fe···Fe distance.

It is not clear why such different conclusions have been reached regarding the importance of Fe···C scattering. It seems unlikely that the carbon shell makes no contribution to the XAFS, particularly for a ligand that is as ordered as tris(pyrazolyl)borate. It is possible that minor variations in the amplitude and phase parameters that were used to fit the data led to major changes in the global minimum (i.e., to changes in the dependence of R_{Fe-Fe} on the presence of a carbon shell). Since **A** is a model compound, the Fe···Fe distance is known independent of the XAFS. For a protein, however, it may not even be known whether or not an Fe···Fe interaction exists. In this case, the model studies suggest that XAFS will be unable to provide a unique determination of whether or not an Fe···Fe interaction is present. However, if an Fe···Fe interaction is known to be present from some other method, the model studies suggest that XAFS can potentially be used to obtain accurate Fe···Fe separations.

The detectability of Fe···Fe scattering is likely to be particularly poor in enzymes such as purple acid phosphatase (PAP), since here it is likely that both Fe···C and Fe···P will contribute to the outer shell XAFS at distances close to the Fe···Fe distance. Although this complicates the analysis, it is also true that if XAFS can be used to reliably detect Fe···P scattering, the Fe···P distance can be very helpful in characterizing the site. Model studies suggest that the Fe···P scattering is
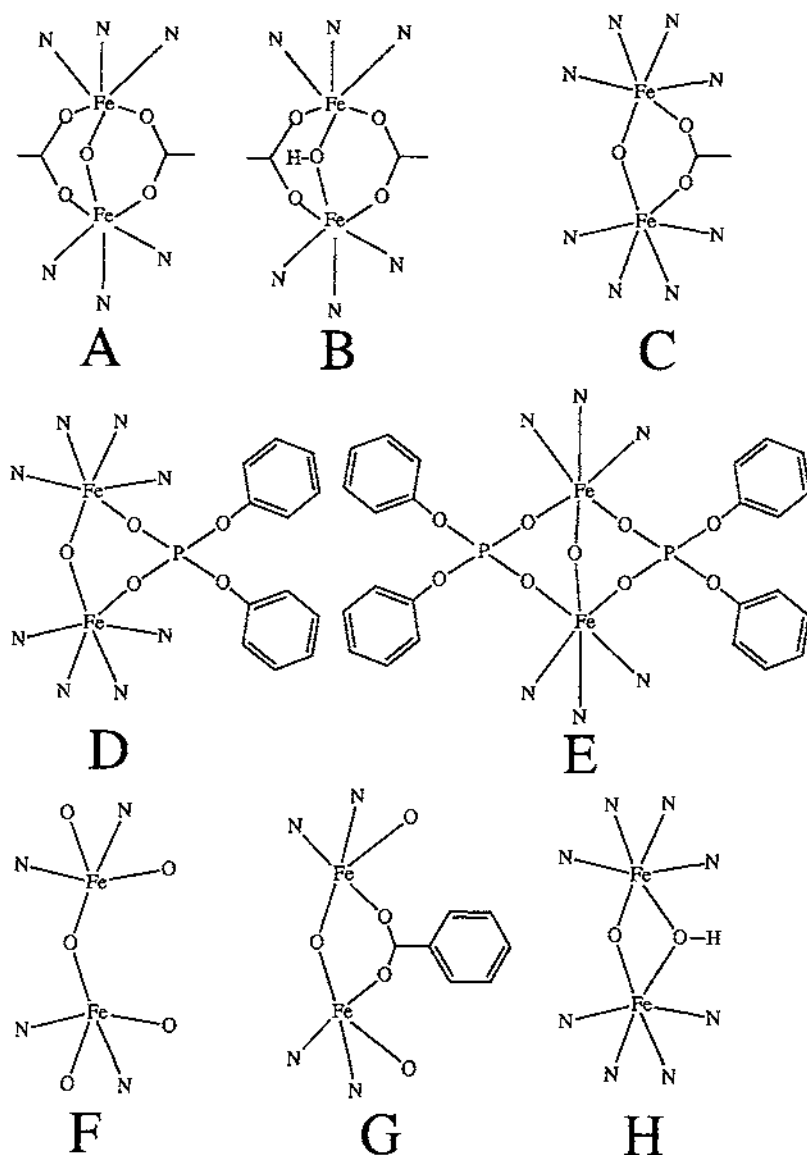
Fig. 6. Schematic illustration of the immediate ligation environment of the Fe models discussed in text.

detectable by XAFS. The XAFS data for $[Fe_2O(OAc)(TPA)_2](ClO_4)_3$, **C**, and $[Fe_2O\{O_2P(OPh)_2\}(TPA)_2](ClO_4)_3$, **D**, (TPA = tris(2-pyridylmethyl)amine) were fit with multiple shells of scatterers [38]. These models differ only in the presence of a carboxylate (**C**) or a phosphate (**D**) bridge. The fits to **D** were much better when a long Fe···P interaction was used rather than an Fe···C shell. As expected, the opposite was true for **C**. The Fe···P distance that was determined for **D** was 3.20 Å

vs. 3.21 Å in the crystal structure. It is important to note, however, that in order to resolve this distance, seven shells of scatterers were used, including Fe···Fe at 3.36 Å, Fe···P at 3.20 Å and Fe···C at 3.03 Å. In another case, fits to $[Fe_2O\{O_2P(OC_6H_5)_2\}_2(HB(pz)_3)_2]$, **E**, were greatly improved by including an Fe···P interaction at 3.23 Å in addition to an Fe···Fe interaction at 3.30 Å [36]. These fits are encouraging in that they illustrate the ability of XAFS calculations to reproduce measured spectra. It is not clear, however, that it would be realistic to include this large a number of scatterers in fits of protein data. This is particularly true if the protein data are noisy and extend over a limited k range. There was not a complete assessment of parameter correlation in these papers. However, it is likely that fit parameters for the Fe···Fe, Fe···P , and Fe···C shells are highly correlated, thus making it difficult to obtain reliable XAFS results in the absence of other structural information.

4.1.2. Identification of bridging ligation

The XAFS spectra of **B** are significantly different from those of **A**, thus indicating the dramatic effect of the short Fe–O interactions from the μ-oxo bridges. The raw XAFS spectra for **A** and **B**, together with that of the hydroxylase component of methane monoxygenase (MMO), are compared in Fig. 7 [39]. The striking similarity of the spectrum of **B** to the spectrum of MMO led to the assignment of μ-hydroxo bridging for this protein (see below).

Although this approach seems to work for **A** and **B**, it is not clear that XAFS is always able to identify uniquely the presence of an oxo bridge. For example, the singly bridged model complex $[N\text{-}(n\text{-propyl})sal)_2Fe]_2O$ (sal = salicylaldiminate), **F**, has 1 Fe–O at 1.78 Å, 2 Fe–O at 1.93 Å, and 2 Fe–N at 2.14 Å. XAFS studies of this complex [35] showed that the data could be fit adequately using only two shells with Fe–O/N distances of 1.90 Å and 2.15 Å. This surprising result was attributed to destructive interference between the 1.78 Å and the 1.93 Å Fe–O interactions. More recently, XAFS spectra have been reported [38] for an equally disordered model complex, $[Fe_2O(OBz)(HDP)_2](BPh_4)$ (where HDP = N-(o-hydroxybenzyl)-N,N-bis(2- pyridylmethyl)amine), **G**, which has a wide distribution of Fe–O/N distances (1.79 Å, 1.93 Å, 2.07 Å, 2.17 Å, and 2.27 Å). As a result of this disorder, the first shell FT peak is greatly reduced in amplitude. A total of four shells of nearest neighbor interactions were used to fit these data, including an oxo shell at 1.79 Å. The authors justified the use of four shells because only in this case could reasonable σ^2 values be obtained. Although the four-shell fits are reasonable when compared to the crystallographic distribution of ligands, there is no significant improvement in the goodness of fit relative to the three- or even the two-shell fits. An estimate of F', based on the fit parameters that are reported in the paper, suggests that the four-shell fit is at least 3-times worse than the two-shell fit.

It is instructive to consider why the oxo bridges that are known to be present in **F** and **G** do not appear to be uniquely identifiable while the oxo bridge in **A** was one of the dominant features of the XAFS spectrum. The differences in ligation between these complexes seem to be primarily responsible for their different XAFS behavior. In **A**, the non-oxo ligands (three pyrazole nitrogens at 2.16 Å + two carb-
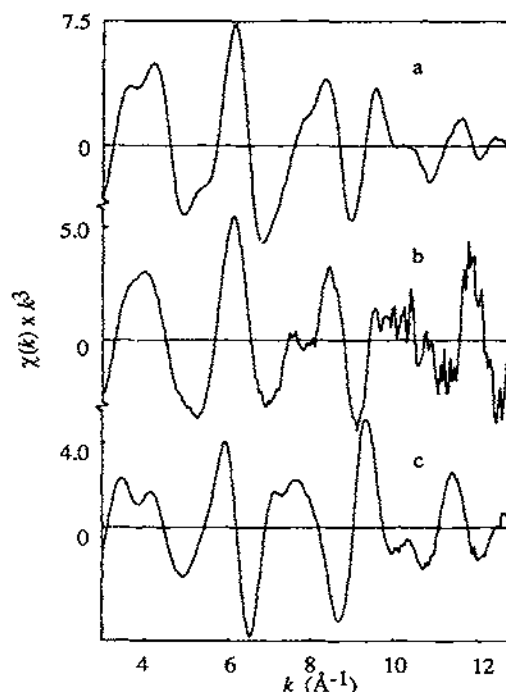
Fig. 7. EXAFS of **A** and **B** compared to that of MMO. (a) Hydroxo-bridged model (**B**). (b) mixed-valence MMO. (c) oxo-bridged model (**A**). Note the significant change in the XAFS on protonating the μ-oxo bridge. The similarity between the MMO spectrum and the spectrum of **B** led to the assignment of μ-OH bridging in MMO. Reproduced with permission from Ref [37].

oxylate oxygens at 2.0 Å) are at relatively long distances from the Fe, and the Fe–O_{oxo} could be resolved. In contrast, the ligation in **F** and **G** includes other short (≈ 1.93 Å) oxygen distances. Under these conditions, destructive interference between the oxo and the other short Fe–O shells makes unique identification of the oxo shell extremely difficult, as predicted by Eq. 8. Similar restrictions are likely to hold in XAFS studies of dinuclear proteins having phenolate ligation. It is important to note that even for **A**, where the oxo and non-oxo shells are reasonably well resolved, the Fe–O_{oxo} interaction was not apparent if the data were fit with only two shells of nearest-neighbor scatterers [40]. For the two shell fits, the shorter Fe–O shell refined to a distance intermediate between the Fe–O_{oxo} and Fe–$O_{carboxylato}$ distances. It was only when three shells of O/N scatterers were used that the short Fe–O distances was resolved. Hedman et al. [40] stress that fits for **A** over a shorter k range (4–12 Å^{-1} vs. 4–16 Å^{-1}) cannot support the resolution of the first shell into three components. A small k range (3–10 Å^{-1}) may similarly be responsible, at least in part, for the lack of observed μ-oxo M–O distances in **F** [35].

Recently, XAFS has been used to distinguish between Fe–O distances arising from a μ-oxo bridge and a μ-hydroxo bridge in a novel μ-oxo,μ-hydroxo bridged dinuclear Fe complex, [Fe2(μ-O)(μ-OH)(6TLA)$_2$](ClO$_4$)$_3$, **H** [41] (6TLA = tris[(6-methyl-2-

pyridyl)methyl]amine). The XAFS analysis of **H** utilized three shells of N/O nearest neighbors at 1.82 Å, 1.99 Å and 2.20 Å. The crystal structure for **H** shows only a single bridging Fe–O distance at 1.91 together with terminal Fe–N distances of ca. 1.98 Å. The long Fe–O bridge distance that is seen in the crystal structure is attributed to an average of a short (i.e., 1.82 Å) Fe–O_{oxo} and a longer Fe–$O_{hydroxo}$ distance. The observation of a short Fe–O_{oxo} distance in the XAFS supports this interpretation. The Fe···Fe separation for **H** was determined to be 2.91 Å from XAFS and 2.94 Å with X-ray crystallography.

4.2. Protein studies

There have been numerous studies utilizing XAFS to characterize dinuclear Fe proteins. For several proteins, high resolution crystal structures have recently become available. These make it possible to determine the extent to which XAFS measurements were able to characterize the Fe···Fe interaction and to identify the bridging ligands. The structural parameters for all of the dinuclear Fe proteins that have been studied by XAFS are summarized in Table 1, together with the high resolution crystallographic results, where available.

4.2.1. Hemerythrin

XAFS spectroscopy has been used to probe the hemerythrin dinuclear iron site in a variety of redox states and in the presence of inhibitors. Deoxyhemerythrin (deoxyHr) and oxyhemerythrin (oxyHr) are the O_2-free, diferrous, and O_2-bound, diferric, forms of the enzyme, respectively. The O_2-free diferric form (metHr) can be prepared with azide (metHrN$_3$) or hydroxide (metHrOH) bound in the vacant oxygen binding site. Finally, an azide bound mixed valent Fe(II)/Fe(III) enzyme (semimetHrN$_3$) is also stable. The presence of Fe···Fe XAFS has been reported for all six forms of the enzyme (see Table 1).

The two initial studies of *Phascolopsis gouldii* metHrN$_3$ both showed the presence of a short Fe–O bond at 1.80 Å that was attributed to a μ-oxo bridge. This was clearly resolvable from longer Fe–(O/N) bonds at an average length of ca. 2.1 Å [42,43]. This general structure has been confirmed by crystallography [44], and the XAFS bond lengths for both the shorter and the longer shells are in excellent agreement with the crystal structure (see Table 1).

In contrast to this success, initial determination of the Fe···Fe distances was less successful. In both studies, the apparent Fe···Fe distance was substantially longer than the distance that was subsequently determined crystallographically [45]. In the first case [42], room temperature data were fit over the k range of 3 to 10 Å^{-1}. The limited k range, together with the use of a less than ideal model compound, $[Fe_3O(glycinato)_6(H_2O)_3](ClO_4)_7$, may be responsible for the error in this case. In the second case [43], the data extended to $k = 16$ Å^{-1} and thus were more likely to give a reliable Fe···Fe distance. In fact, the authors initially obtained a distance that was close to the (subsequently determined) crystallographic value. However, the authors increased their estimate of the Fe···Fe distance by ≈0.15 Å to 3.38 Å in an

Table 1
XAFS data analyses for dinuclear iron metalloproteins[a]

Sample	M–O (bridge)		M-(O/N)		M (O/N)[b]		M···M		k range (Å^{-1})	Temp. (K)	Year	Ref.
	R (Å)	CN	R (Å)	CN	R (Å)	CN	R (Å)	CN				
HR												
metHrN₃	1.80	1.0	2.15	5.0			3.49	1.0	3.0–10.5	300	1982	42
	1.76	1.0	2.07	2.3	2.13	2.2	3.38	2.0	4.0–16.0	300	1982	43, 47
							3.20c	1.0			1986	40
	1.80	1.0	2.13	5.0	2.17	3.0	3.19	1.0	4.0–14.3	77	1986	37, 48
	1.80	1.0	2.08	2.0			3.24	1.0	3.2–11.0	80	1988	49
	1.77	1.0	2.24	5.0			3.25	1.0	crystal		1983	46
	1.80	1.0	2.19	5.0			3.23	1.0	crystal		1991	44
metHrOH	1.82	1.0	2.15	5.0			3.54	1.0	3.0–10.5	300	1982	42
							3.2–3.4d	1.0	crystal		1982	52
oxyHr	1.83	1.0	2.16	5.0			3.57	1.0	3.0–10.5	300	1982	42
	1.82	1.0	2.11	2.5	2.22	2.5	3.24	1.0	2.5–12.0	80	1988	49
	1.84	1.0	2.18	5.0			3.27	1.0	crystal		1991	51
metHr	1.82	1.0	2.07	2.0	2.14	2.5	3.13	1.0	2.5–12.0	80	1988	49
	1.79	1.0	2.17	4.5			3.21	1.0	crystal		1983	46
	1.79	1.0	2.14	4.5			3.25	1.0	crystal		1991	44
semimetHrN₃	1.87	1.0	2.14	5.0			3.46	1.0	3.5–14.3	77	1987	48
deoxyHr			2.02	3.0	2.14	2.5	3.13	1.0	3–9.75	80	1983	50
	1.98	1.0	2.12	2.4	2.25	2.5	3.57	1.0	2.5–12.0	80	1988	49
	2.02	1.0	2.21	5.0			3.32	1.0	crystal		1991	51

Protein	Form	R	CN	R	CN	R	CN	R(Fe···Fe)	CN	k-range[b]	T	Year	Ref
RR	B₂	1.80	1.0	2.06	5.0			3.22	1.0	4.0–14.3	77	1986	37
		1.80	1.0	2.06	5.0			3.22	1.0	3.5–14.3	77	1987	48
		1.78	1.0	2.04	5.0			3.26–3.48	1.0	2.8–8.5	200	1987	53
		2.0	*1.0*	*2.20*	*5.0*			*3.35*	*1.0*	*crystal*		1993	54
	metB₂	1.78	1.0	2.06	5.0			3.19	1.0	4.0 14.3	77	1986	37
		1.78	1.0	2.06	5.0			3.19	1.0	3.5–14.3	77	1987	48
		1.78	1.0	2.04	5.0			3.26 3.48	1.0	2.8–8.5	200	1987	53
MMO	oxidized			1.92	4 6	2.14	2.3	3.05	1.7	4.0 10.5	4.2	1988	55
			–	1.97	3.5			3.42	1.1	4.0–12.0	10	1991	57
	as-isolated							3.4[d]	1.0	crystal		1993	58
	semimet		–	1.99	3.5	2.20	2.0	3.43	1.0	3.5–12.2	10	1988	39
				2.00	3.4	2.21	2.6	3.42	1.1	4.0–12.0	10	1991	57
			–	1.95	2.6	2.15	3.0	3.41	1.3	4.0–12.0	10	1991	57
	reduced			2.15	5.1					4.0 12.0	10	1991	57
PAP	oxidized·PO₄	–		1.98	3.0	2.15	3.0	3.00, 3.06[e]	0.6, 1.0[e]	1.0–12.0	193	1986	36
		1.94	1.5	2.10	3.5	2.44	1.0	3.22, 3.17[e]	1.0, 1.0[e]	2.5–13.0	100	1993	38
	oxidized·AsO₄	1.96	1.5	2.12	3.5	2.45	1.0	3.29, 3.41[e]	1.0, 1.0[e]	2.5–13.0	100	1993	38
	mixed valence	–	–	2.01	3.0	2.17	3.0	–	–	1.0–11.0	193	1986	36
		1.93	1.5	2.14	3.5	2.34	1.0	3.52	1.0	2.5 13.0	100	1993	38

[a] Distances (R) and apparent coordination numbers (CN) from XAFS analysis. The corresponding average values from crystal structures are given in italics where available.

[b] This column gives distances for the third nearest neighbor shell when this shell was included in the XAFS refinement.

[c] Re-determination of the Fe···Fe distance given in the previous line is based on an improved interpretation of multiple scattering.

[d] Refined Fe–ligand distances have not yet been reported.

[e] Parameters for the Fe···P and Fe···As shell.

attempt to account for the multiple scattering that was expected to exist in the $Fe_2(\mu\text{-}O)$ core.

Soon after the initial XAFS structures appeared, the 2.0 Å resolution crystal structure was reported for metHrN$_3$ [46]. This showed an Fe···Fe distance of 3.25 Å, which is substantially shorter than that found by either XAFS study. Subsequent detailed analysis of the outer shell XAFS of μ-oxo bridged Fe$_2$ models showed that the multiple-scattering effects are less important than had originally been thought [36]. In particular, multiple scattering effects become negligible as the Fe–O–Fe bond angle decreases below 150° and thus should not affect the XAFS of metHrN$_3$. This led to the conclusion that the 0.15 Å correction [47] should not have been made, and thus that 3.20 Å is the correct Fe···Fe separation [36], in good agreement with the crystal structure. Several subsequent studies have all confirmed this conclusion [37,48,49]. In other words, once it had been established crystallographically that the Fe–O–Fe unit was bent, XAFS analysis was able to give a reliable Fe···Fe distance. The latter is not a trivial point. Although crystallography was essential for establishing the $Fe_2(\mu\text{-}O)$ core geometry, crystallography is not a particularly good technique for determining precise bond lengths. Typical estimates of the uncertainties in XAFS distances are 5–10-times smaller than the uncertainties in most protein crystal structure bond lengths. The agreement among the recent (post 1983) XAFS studies is good (see Table 1), thus demonstrating the reliability (or at least reproducibility) of XAFS distances once the basic structural motif has been established.

There is one variation among the XAFS studies that deserves comment. For many studies, the first shell data were modeled by a short Fe–O$_{oxo}$ and a longer Fe–(O/N) shell. However, in two cases the Fe-ligand scattering was refined in three shells, with the two outer shells representing Fe–O$_{carboxylato}$ and longer Fe–N$_{imidazole}$ distances [43,47]. If the published F values are used to estimate F', it appears that there was substantial improvement in F' when the second shell was included. However, addition of the third shell does not appear to be justified as judged by F'. Consistent with this, the refined Fe–O and Fe–N distances in the three-shell model are very similar and their average is always very close to the refined Fe–(O/N) distance in the two shell model. These two different models thus provide equivalent structural information. It is unlikely that XAFS could have been used to demonstrate the presence of distinct Fe–O$_{carboxylato}$ and Fe–N$_{imidazole}$ shells in the absence of crystallographic evidence that they must be present. Given that both Fe–O and Fe–N shells are present, it is possible to refine their average distances. The resulting distances are chemically reasonable, although it is likely that the refined Fe–O$_{carboxylate}$ and Fe–N$_{imidazole}$ distances are highly correlated. An alternative approach to resolving the first shell distances is described below in the discussion of urease.

XAFS analyses of oxyHr and metHr proteins showed core structures very similar to that seen in metHrN$_3$, with a shell of short Fe–O bonds and a second shell of Fe–(O/N) scatterers at a longer distance [42,49]. Based on the intensity of the $1s \rightarrow 3d$ transition in metHr, it was suggested that there is a vacant coordination site on a single Fe in this derivative [49]. This was subsequently confirmed by the crystal structure [44]. The 1982 study of oxyHr, published before the 2.0 Å resolution crystal structure appeared, gave an apparent Fe···Fe distance of 3.57 Å, substantially

longer than the Fe···Fe distance that was subsequently found crystallographically for metHr [46]. However, a later XAFS study at 80 K gave an Fe···Fe distance that is consistent with the crystal structure [49].

The XAFS data for metHr gave an apparent Fe···Fe distance of 3.13 Å. This is somewhat shorter than the most recent crystallographic Fe···Fe distance [44]. However, within uncertainty, these two are probably not distinguishable. An unusual feature of the metHr crystal structure is the presence of two very different Fe-O_{oxo} distances of ca. 1.66 and 1.92 Å. Structural studies of oxo bridged Fe models and resonance Raman studies of hemerythrin appear to be inconsistent with such asymmetry [44]. In addition, no evidence for this asymmetry is seen in the XAFS. Instead, the XAFS data give an Fe-O_{oxo} distance that is equal to the average of the two crystallographic bond lengths. If there were an Fe-O_{oxo} distance of 1.66 Å, this should be detectable by XAFS. It remains to be seen whether there is in fact an asymmetry in the Fe-O_{oxo} distances that XAFS has missed or whether there is a small error in the refined crystallographic position of the bridging oxo ligand.

The initial XAFS analysis of deoxyHr at 300 K failed to identify an Fe···Fe feature analogous to that seen for the ferric forms of the enzyme [42]. Subsequent measurements at 80 K on data to $k = 9.75$ Å^{-1} were interpreted in terms of an Fe···Fe interaction at 3.13 Å. This suggested that although the Fe_2 core was different from that in oxyHr, the core was still intact [50]. First shell analysis showed no evidence for a short Fe-O bond at ca. 1.80 Å. The data were still fit using two shells; however, the "short" Fe-O shell refined to a substantially longer distance of 2.02 Å. A third study by this same group extended the XAFS data to $k = 12.0$ Å^{-1} [49]. With these data, the apparent Fe···Fe separation increased by 0.4 Å to 3.57 Å. The authors suggested that this discrepancy was the result of the inappropriate use of [$Fe_3O(glycinato)_6(H_2O)_3$])ClO$_4$)$_7$ as a standard in the earlier study. An alternative explanation for the difference is that the longer k range of the later study changes the global minimum from one with an apparent Fe···Fe distance of 3.1 Å to one with an apparent Fe···Fe distance of 3.6 Å. In this study, the Fe-nearest neighbor bonds were fit with three shells of Fe-O/N scatterers at 1.98 Å, 2.12 Å, and 2.25 Å. As discussed previously, it is extremely difficult to resolve distances this close using XAFS data over such a limited k range. However, these data are nevertheless consistent with the earlier XAFS studies showing that there is no short Fe-O distance in deoxyHr. This suggested that the μ-oxo bridge in oxyHr is protonated in the deoxyHr enzyme.

Subsequent to these XAFS studies, the 2.0 Å crystal structure of deoxyHr was published, giving an Fe···Fe separation of 3.32 Å [51]. It thus appears that none of the XAFS studies of deoxyHr have given an Fe···Fe distance within 0.2 Å of the crystallographic value. This is larger than the estimated errors of the two techniques. It is not clear at this point whether the crystallographic distance or the most recent XAFS distance is correct.

Finally, XAFS data have been analyzed for metHrOH [42] and semimetHrN$_3$ [48]. First shell analyses for both systems are consistent with Fe(III)$_2$(μ-O) and Fe(II)/Fe(III)(μ-OH) cores, respectively, as expected based on the known chemistry of Hr. The apparent Fe···Fe separations are larger than that seen in the deoxyHr

crystal structure and in the low resolution crystal structure of metHrOH [52]. These long distances seem unlikely to be correct, particularly for metHrOH, which would be expected to be quite similar to metHrN$_3$. However, high resolution crystal structures are not yet available to test this point.

The track record for XAFS in characterizing hemerythrin is thus rather mixed. On the one hand, all of the first shell XAFS analyses are consistent with the crystal structure distances (aside from differences of opinion regarding how many shells of scatterers can be resolved). In all cases, the first shell XAFS analyses appear to have correctly identified the bridging ligation as μ-oxo or μ-hydroxo in advance of the crystal structures. On the other hand, with the possible exception of semimetHrN$_3$, none of the XAFS analyses has given the correct Fe···Fe distance prior to crystallographic characterization. In the case of metHrN$_3$, this was due to misinterpretation of multiple scattering contributions [47]. In the other cases, the errors may have resulted from interference between Fe···C and Fe···Fe XAFS. Most of the "pre-crystallography" XAFS measurements were made at 300 K, where the Fe···Fe XAFS signal is expected to be weak. If the Fe···Fe signal is small in comparison to the Fe···C signal, it may be possible to interpret the Fe···C$_{imidazole}$ XAFS as an apparent Fe···Fe interaction at ca. 3.5–3.6 Å. This would be consistent with the Fe···Fe/Fe···C ambiguity that has been found in model compound studies [36]. For deoxyHr, the XAFS measurements were later repeated at 80 K, but still seem to have given the incorrect Fe···Fe distance. One possibility is that protonation of the oxo bridge in deoxyHr weakens the Fe···Fe interaction to the point that it remains XAFS non-detectable, at least down to 80 K. In this case, the apparent 3.57 Å Fe···Fe distance could again be the result of attributing Fe···C scattering to an Fe···Fe interaction. Of course, another possibility is that the 2.0 Å crystal structure gives an erroneously short Fe···Fe distance. Low temperature (ca. 4 K) XAFS measurements and/or a higher resolution crystal structure will be required to distinguish between these possibilities.

4.2.2. Ribonucleotide reductase

Two groups have reported XAFS characterization of the Fe$_2$ core in the R^2 subunit (formerly known as the B$_2$ subunit) of *E. coli* ribonucleotide reductase [37,48,53]. Both the native diferric form (R$_2$) and the tyrosine reduced (metR$_2$) form have been studied. The different XAFS results are in good agreement with one another and both studies suggest that there are no significant changes in structure when the tyrosine radical is reduced.

All of the XAFS analyses showed the presence of a short Fe–O bond at ca. 1.79 Å and a second shell of 5 Fe–(O/N) scatterers at ca. 2.06 Å. Based on the observation that the Fe–(O/N) nearest neighbor distance was shorter than that in metHrN$_3$, it was suggested that R$_2$ contains fewer histidine ligands, with an estimate of three per Fe$_2$ core. One study, using data from 3.5–14.3 Å^{-1}, found an Fe···Fe component at 3.22 Å, low Z scatterers at ca. 3.03 Å, and a second shell of low Z scatterers at ca. 4.30 Å [37,48]. In a second study, using a k range of 3–9 Å^{-1} [53], the Fe···Fe interaction was estimated to be between 3.26 and 3.48 Å. This large range was based on the earlier observations (see above) that multiple scattering contributions can

cause an apparent decrease in the Fe···Fe distance of up to 0.22 Å [47]. As described above, it is now recognized that multiple scattering is not particularly important for Fe–O–Fe angles less than 150°; thus the lower limit of this range (≈ 3.26 Å) appears most reasonable. With this adjustment, the two independent studies suggest very similar core structures.

Recently, the 2.2 Å crystal structure for ribonucleotide reductase has been reported, providing a test of the XAFS results [54]. The crystallographic Fe–(O/N) distance is 2.16 Å and the Fe···Fe separation is 3.35 Å. The differences between the crystallographic and XAFS Fe···Fe distances are 0.09–0.13 Å. Although this difference is substantially larger than the estimated uncertainty of the XAFS, it is probably within the uncertainty of the present crystal structure. It remains to be seen whether future crystallographic refinements will converge to a shorter Fe···Fe distance (i.e., a case where XAFS has predicted the correct structure in advance of the crystallographic determination), or whether this will turn out to be another case where the apparent XAFS Fe···Fe distance has been perturbed by Fe···C scattering.

4.2.3. Methane monooxygenase

XAFS spectroscopy has been used to characterize the reduced, Fe(II)/Fe(II), the mixed valence, Fe(II)/Fe(III), and the oxidized, Fe(III)/Fe(III), derivatives of methane monooxygenase (MMO). Initial XAFS studies focused on the oxidized protein. Data for MMO were measured over a very limited k range (ca. 4–10 Å^{-1}). These data were interpreted in terms of an average Fe–(O/N) bond length of 1.92 Å and an Fe···Fe separation of 3.05 Å [55]. With this limited k range, the authors were unable to resolve any detail within the first shell. However, they concluded that the short Fe···Fe distance required the presence of either a μ-O or a μ-OH bridge. Since crystallographically characterized μ-OH bridges typically have Fe–O distances of ca. 1.9 Å with even longer terminal Fe–(N/O) distances, it is hard to imagine how the average first shell distance in MMO could be 1.92 Å without the presence of a μ-O bridge.

At about the same time, an attempt was made to measure XAFS data for the oxidized enzyme from *Methylococcus capsulatus* (BATH). In this case, the protein was found to undergo photoreduction, to give the mixed-valence Fe(II)/Fe(III) species which was then stable with respect to further photoreduction [39]. XAFS data for the mixed valence form were adequately fit with two shells of Fe–(O/N) scatterers at distances of 1.99 Å and 2.20 Å, an Fe···Fe shell at 3.42 Å and an Fe···C shell at 3.27 Å [56]. The data extended to high enough k that it should have been possible to resolve an Fe–O$_{oxo}$ shell, if one was present. The absence of a short Fe–O shell at ca. 1.80 Å together with the observation of a long Fe···Fe separation of 3.42 Å, suggested that mixed-valence MMO has a μ-hydroxo bridged Fe$_2$ core.

Recent measurements on a photoreduction insensitive preparation of the oxidized enzyme gave a shell of 3.5 Fe–(O/N) scatterers at 1.97 Å and a second shell of 2.3 Fe–(O/N) scatterers at 2.14 Å [57], suggesting that, at least in this preparation, the oxidized dinuclear core has a μ-OH rather than a μ-O bridge. This study also addressed the difficulties of defining Fe···Fe interactions in the presence of Fe···(C/N) scattering. The authors report an Fe···Fe separation of 3.42 Å. However, they note

that this value was obtained only when an $Fe_2(\mu\text{-OH})$ standard was used to describe the $Fe\cdots Fe$ scattering. The difficulty here should be obvious. In order to choose the correct model, it is necessary to know the identity of the bridging ligand. If a μ-O interaction is seen in the XAFS, an $Fe_2(\mu\text{-O})$ model can be used. However, it has been shown for model compounds (see above) that some μ-O bridged dimers lack resolvable short $M-O_{oxo}$ signals. This means that the lack of an XAFS detectable oxo bridge does not necessarily rule out an $Fe_2(\mu\text{-O})$ core in oxidized MMO. However, in the case of MMO, the latter XAFS results have recently been confirmed by a 2.2 Å crystal structure [58]. The crystal structure for as-isolated MMO (believed to be in the oxidized form) is consistent with an $Fe_2(\mu\text{-OH})$ structure with an $Fe\cdots Fe$ distance of 3.4 Å.

It is not clear why such dramatically different results have been obtained in XAFS studies of oxidized MMO. The early $Fe\cdots Fe$ distance of 3.04 Å is significantly shorter than the distance found in the most recent XAFS and in the crystal structure. In addition, the first shell distance in the initial work (1.92 Å) is significantly shorter than that found in the later XAFS work and in the crystal structure. It may be that these differences reflect genuine structural differences in MMO from different species. It seems more likely, however, that these differences reflect the difficulty of extracting structural parameters from noisy XAFS data that extend over a very limited k range.

A more recent study of mixed valence MMO [57] has confirmed the result found in the initial study of X-ray photoreduced enzyme. The average $Fe-(O/N)$ bond length is between 2.06 and 2.09 Å, with no detectable $Fe-O_{oxo}$ shell. This $Fe-(O/N)$ bond length represents an increase of 0.02–0.05 Å relative to the oxidized enzyme, as expected for reduction of one Fe from Fe(III) to Fe(II). The apparent $Fe\cdots Fe$ separation is 3.41–3.43 Å for both of the mixed valence samples, suggesting that the Fe_2 core in the mixed-valent enzyme is very similar to that in the oxidized enzyme. This would be consistent with the presence of a μ-OH rather than a μ-O bridge in both oxidation states. Further reduction of MMO to the diferrous form results in a further increase of the average $Fe-(O/N)$ bond length to 2.15 Å and the loss of any detectable $Fe\cdots Fe$ XAFS signal [57].

The detectability of $Fe\cdots Fe$ XAFS has been analyzed in detail for MMO [57]. Of particular importance is the finding that there exists an alternative fit minimum with an apparent $Fe\cdots Fe$ separation of ca. 3.0 Å. This appears to be due to the fact that there are contributions from both Fe and C scatterers in the range $R = 3.0\text{–}3.4$ Å. The refined parameters for these shells are strongly correlated, thus leading to the possibility of a false minimum at an $Fe\cdots Fe$ distance of ca. 3.0 Å.

4.2.4. Purple acid phosphatase

XAFS spectroscopy has been used to study the purple acid phosphatases isolated from bovine spleen (BSPAP) and porcine uterine fluid (uteroferrin, Uf). The enzymes have been studied in the Fe(II)/Fe(III) mixed valent form (BSPAP$_r$ and Uf$_r$), in the phosphate inhibited diferric form (BSPAP$_o\cdot PO_4$ and Uf$_o\cdot PO_4$), and, for uteroferrin, in the arsenate inhibited diferric form (Uf$_o\cdot AsO_4$).

The initial analysis of BSPAP$_o\cdot PO_4$ XAFS data measured at 193 K utilized two shells of $Fe-(O/N)$ scatterers at 1.98 and 2.15 Å, a third shell of 0.6 $Fe\cdots Fe$ scatterers

at 3.00 Å, a fourth shell which was best simulated with a single Fe···P scatterer at 3.06 Å, and a fifth shell for the Fe–(C/N) imidazole interactions at 4.3 Å [35]. The short Fe···Fe separation, coupled with NMR, resonance Raman, and magnetic susceptibility data, suggested the presence of several bridging ligands, including either a μ-oxo or μ-hydroxo bridge. No resolvable Fe–O_{oxo} shell was seen. However, the authors noted that this does not necessarily rule out the possibility of oxo ligation. A more recent study [38] of $Uf_o \cdot PO_4$ XAFS data measured at 100 K gave significantly different results. In this case, the nearest neighbor interactions were modeled with three shells of Fe–(O/N) scatterers at 1.94, 2.10, and 2.44 Å. The 2.44 Å shell was attributed to the carbon atom from a monodentate carboxylate or the oxygen of an asymmetrically chelated carboxylate. In both studies, only a limited k range was available, thus making it likely that the refined Fe–nearest-neighbor parameters are highly correlated. It is noteworthy that the average Fe–ligand distances in both cases are very similar (2.05–2.07 Å). It is not clear which model, if either, correctly describes the distribution of Fe–nearest neighbor distances. It does seem, however, that both models describe the same average Fe–ligand environment.

In contrast to the general agreement of the first shell results, the outer shell analyses in the two studies are significantly different. The more recent study [38] reported an Fe···Fe shell at 3.22 Å (vs. 3.00 Å in the early study) and a Fe···P shell at 3.17 Å (vs. 3.06 Å in the early study). These differences may reflect structural differences between the enzymes isolated from different organisms. Alternatively, they may reflect a more general multiple minimum problem in XAFS. Contributions are expected from at least three shells (Fe···C , Fe···Fe, and Fe···P) over the R range 3–3.5 Å. If we use $\Delta k = 11$ Å^{-1} and make the generous assumption that the XAFS contributions from these shells extend over $\Delta R = 1$ Å, this still only gives $N_{idp} \leqslant 9$. Given three shells, each of which requires at least R, N, and σ^2 to be defined, we would anticipate that unambiguous assignment of the global minimum will be difficult.

In order to improve the reliability of the analysis, the Uf data were also measured for $Uf_o \cdot AsO_4$ [38]. This experiment should allow identification of the Fe···P signal, since this is the only feature that is expected to change significantly relative to $Uf_o \cdot PO_4$. In comparison with the $Uf_o \cdot PO_4$ data, the Fourier transform of the $Uf_o \cdot AsO_4$ data shows much greater intensity at $R + \alpha \approx 3$ Å. The XAFS refinements for $Uf_o \cdot AsO_4$ showed a slight (0.02 Å) increase in all of the first shell bond lengths, a modest (0.07 Å) increase in the Fe···Fe distance, and a substantial (0.24 Å) increase in the Fe···P/As distance. Here again, multiple minima problems are expected, with the additional complication that Fe···Fe and Fe···As contributions should be difficult to distinguish. The increase in the apparent Fe···(P/As) distance is somewhat surprising, given that As–O bonds are only ca. 0.13 Å longer than P–O bonds [59,60]. This may indicate either an error in the Fe···P and/or Fe···As distance, or a change in geometry for $Uf_o \cdot PO_4$ vs. $Uf_o \cdot AsO_4$. The refined values for the Fe···Fe and Fe···(P/As) distances were used to support a model in which the oxyanion binds to the di-iron core in a bidentate bridging geometry [38].

XAFS data for mixed valence $BSPAP_r$ were measured at 193 K [35]. These data again showed no evidence for a short Fe–O_{oxo} shell. The nearest neighbor scattering

was fit with two shells of Fe–(O/N) at 2.01 and 2.17 Å. No evidence was found for an XAFS detectable Fe···Fe interaction in the BSPAP$_r$. More recently, data have been measured at 100 K for mixed-valence Uf$_r$. The first shell was modeled using a different set of scatterers (Fe–(O/N) at 1.93, 2.14 and 2.34 Å) than in the earlier study of BSPAP$_r$. As with the oxidized enzyme, the two different studies of the mixed-valence enzyme give very nearly the same average Fe–(O/N) distance. The outer shell data for Uf$_r$ were fit with an Fe···Fe shell at 3.52 Å and an Fe···C shell at 3.2 Å. As with mixed valence MMO, there was another minimum with a short Fe···Fe (3.16 Å) and a longer Fe···C (3.54) distance. The former (short Fe···C/long Fe···Fe) was preferred based on the overall goodness of fit. Moreover, the longer Fe···Fe seems most consistent with the absence of an oxo bridge.

There are as yet no crystallographic data available that can be used to determine which of the XAFS models for the purple acid phosphatases are correct. One intriguing observation is the fact that long, ca. 3.5 Å, Fe···Fe distances have been reported previously in 300 K XAFS studies of Hr and for XAFS of deoxyHr. These are all cases where the Fe···Fe XAFS is expected to be weak, and in all of these cases, subsequent crystallographic and/or XAFS analyses have suggested that the apparent 3.5 Å Fe···Fe distance was an artifact. An apparent Fe···Fe distance at ca. 3.5 Å may turn out to be a consequence of the Fe···Fe/Fe···C interference that can occur when fitting XAFS data for Fe-imidazole proteins. Alternatively, uteroferrin may turn out to be the first authentic example of a genuine 3.5 Å Fe···Fe distance. It will be interesting to watch the development of the purple acid phosphatase structure as further studies are undertaken.

5. Manganese XAFS

5.1. Model studies

Manganese model chemistry has provided insight into the structures of the tetra-manganese site in the photosynthetic oxygen evolving complex (OEC) and the di-manganese site in Mn catalase. One feature that appeared in the earliest studies of the OEC [61] and which has persisted to date is the presence of a 2.7 Å Mn···Mn interaction. Much of the model effort has thus been focused on structures containing this feature [62].

As with iron model chemistry, Mn···Mn distances depend on the bridging ligands [63]. The ca. 2.7 Å distance is characteristic of a di-μ-oxo bridged pair, while longer distances are found on protonation of the di-μ-oxo bridged core. A single protonation of the compound [MnIV(μ-O)salpn]$_2$, I [64] (see Fig. 8), results in an increase of 0.10 Å in the Mn···Mn distance from 2.73 Å to 2.83 Å [65]. In the doubly protonated complex, the Mn···Mn distance increases another 0.10 Å to 2.93 Å [66]. This correlation suggests that the Mn···Mn distance can be used to define the bridging ligation.

The ability to distinguish between oxo and hydroxo bridging by using the Mn···Mn distance is important since the Mn–O$_{oxo}$ shell is not necessarily resolvable. The XAFS data for compound I and IH$^+$ do not show a resolvable short Mn–O distance [66], despite the presence of two crystallographically characterized oxo bridges at
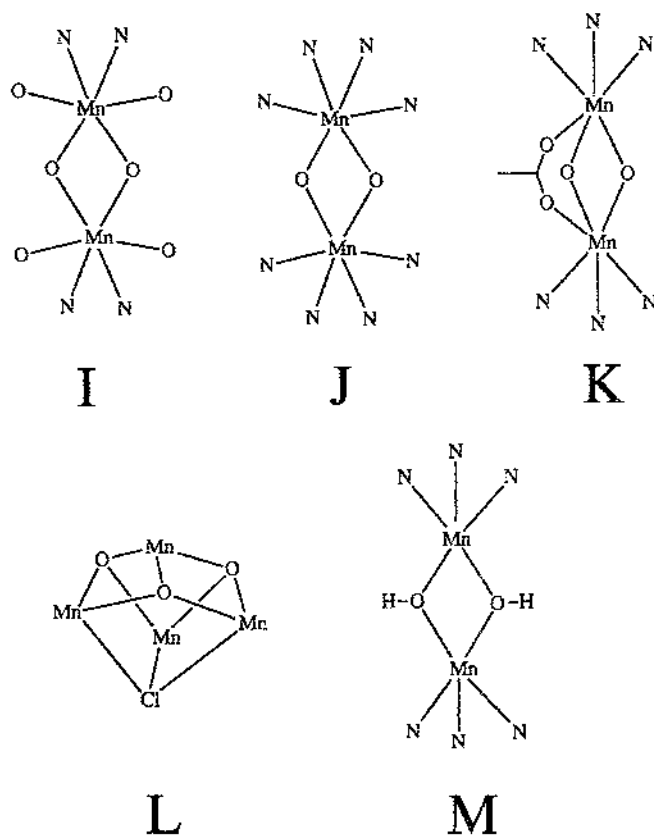
Fig. 8. Schematic illustration of the immediate ligation environment of the Mn models discussed in text.

1.8 Å from the Mn in **I**. This is attributed to the presence of a broad distribution of Mn–(O/N) distances, and in particular to the presence of Mn–$O_{phenolato}$ distances at ca. 1.93 Å. It is probably also important that Mn XAFS spectra are limited, at least for proteins, to $k_{max} \leqslant 11.5$ Å^{-1} due to the Fe K edge jump at 7100 eV. The limited k range makes resolution of multiple shells even more difficult for Mn than it is for Fe.

Despite these difficulties, there are several cases in which short Mn–O_{oxo} shells can be resolved. These complexes have primarily nitrogen terminal ligands, and thus have a more clearly defined two-shell distribution than is found in **I**. Examples include di-μ-oxo-tetrakis(2,2′-bipyridine)dimanganese(III,IV), **J**, and $LMn^{III}(O)_2(OAc)Mn^{IV}L$, **K**, where L = tris[(3,5-di-isopropyl)pyrazolyl]borate. The Fourier transforms of **I**–**K**, the OEC, and Mn catalase are compared in Fig. 9 and the filtered first shell XAFS data are compared in Fig. 10. It is clear qualitatively that there is significant destructive interference between the Mn–O_{oxo} and Mn–(O/N) shells in **J**, **K**, and the Mn catalase. This can be seen both in the presence of split peaks with reduced amplitude in the Fourier transforms (Fig. 9) and in the beat
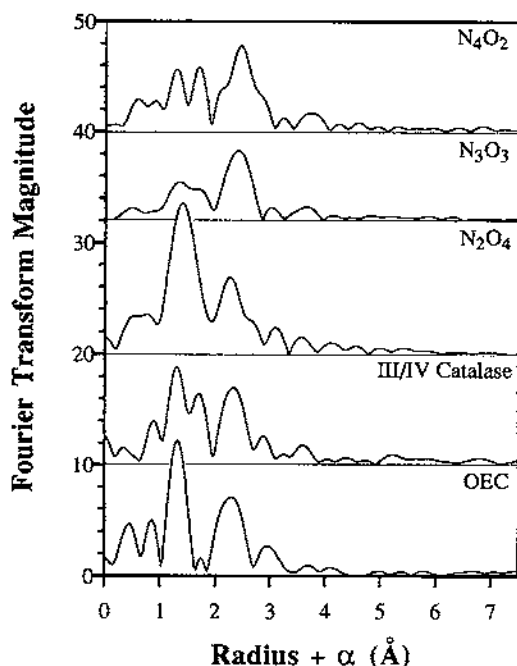
Fig. 9. Fourier transforms of (from top to bottom) I, J, K, superoxidized Mn catalase and the OEC. For J, K and the Mn catalase, the nearest neighbor scattering is partially resolved into an $Mn-O_{oxo}$ and a longer $Mn-(O/N)$ shell. This destructive interference leads to a significant loss of amplitude for these spectra. Transforms calculated for $k = 1.5–11.5$ Å^{-1} using k^3 weighted data.

node in filtered first shell data (Fig. 10). In contrast, the data for I and for the OEC have a single intense first shell peak in the Fourier transform and no obvious beat in the filtered XAFS. This is consistent with the lack of a well defined shell of long $Mn-(O/N)$ bonds in I, and presumably in the OEC [66,67].

One of the striking features of Mn model XAFS in comparison with Fe model compounds is the ease with which the 2.7 Å Mn···Mn feature can be identified. In contrast, there are many examples in the dinuclear Fe literature (see above) in which it is difficult or impossible to distinguish between Fe···C and Fe···Fe scattering. Two features contribute to the success of XAFS in the Mn case. One is the simple absence of Mn···C scattering at distances which can cause interference. As with Fe, the most important interference will come from the outer shells of imidazole ligands. These should appear at $R \geqslant 3$ Å, and thus are not likely to interfere with detection of Mn···Mn scattering at ca. 2.7 Å. The second difference between Mn and Fe models is the prevalence of two single atom bridges (e.g., μ-oxo, μ-hydroxo, μ-phenoxo, etc.) in Mn chemistry. These are likely to give a much more rigid Mn···Mn interaction, and thus lead to significantly enhanced XAFS oscillations in comparison with the oxo-, carboxylato-bridged Fe structures. Indeed, the 2.7 Å Mn···Mn peak is a dominant feature of the XAFS for the Mn models (see Fig. 9), while the 3.3 Å Fe···Fe feature in oxo-, carboxylato-bridged Fe dimers is relatively small. Consistent with
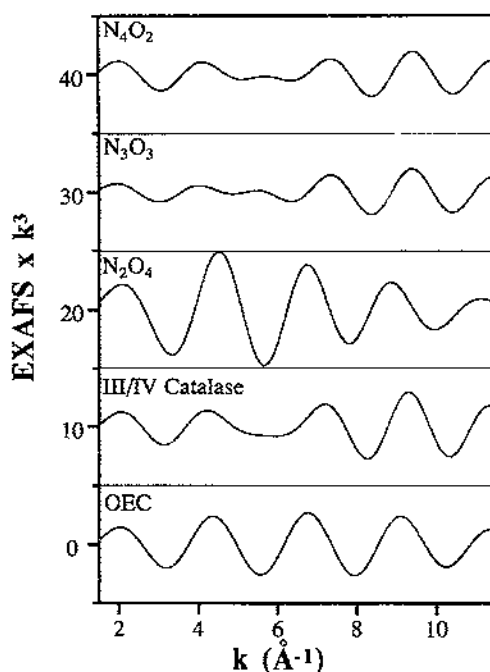
Fig. 10. Filtered XAFS data of the first peak of (from top to bottom) I, J, K, superoxidized Mn catalase and the OEC. A beat node indicating a second frequency is clearly present for J, K and the Mn catalase, but not for I or the OEC. Filters calculated over $R + \alpha \approx 1$–2 Å.

this, the $(\mu\text{-}O))(\mu OH)$ bridged Fe dimer, H, showed an intense, unambiguous Fe$\cdots$Fe interaction (see above) [41].

In addition to the 2.7 Å features, there are other, longer distance interactions in the OEC (see below). Furthermore, it is known from biochemical studies [68] that Ca(II) and Cl$^-$ are required co-factors for oxygen evolution. Thus, there has been much interest in determining whether XAFS can be used to detect Mn–Cl, Mn$\cdots$Ca and long Mn$\cdots$Mn interactions. In a recent study [69], several Mn dimers, trimers and tetramers were analyzed to address this question. One model was $[Mn_4O_3Cl(OAc)_3(dbm)_3]$, L, which has a distorted cubane structure with a μ_3-chloride bridge. The crystallographic Mn–Cl distances range from 2.64 Å to 2.66 Å and could be adequately modeled with an apparent Mn–Cl distance of 2.61 Å. The presence of a 2.8 Å Mn$\cdots$Mn distance did not interfere with the Mn–Cl fitting. However, the longer Mn$\cdots$Mn interactions at 3.25 Å could not be modeled in the XAFS unless the distances and coordination numbers were constrained to the known crystallographic values. Without these constraints, the longer Mn$\cdots$Mn shell refined to 2.99 Å. It seems likely that this is due to interference between the long Mn$\cdots$Mn and the Mn$\cdots$C shells at approximately the same distance. For other model compounds, the filtered XAFS data could be adequately simulated if multiple shells were used [69]. As with several of the Fe model compounds, this demonstrates the ability of modern XAFS parameters to verify known structures.

For many of these fits the number of variables appears to exceed the number of degrees of freedom. Thus, it is not clear that this fitting protocol can be used to determine unknown structures.

With the exception of **L**, the models discussed above did not show evidence for interference between Mn···Mn and Mn···C shells. In contrast, the XAFS data for a Mn(II) dimer, [Mn(HB(3,5-iPr$_2$pz)$_3$]$_2$(OH)$_2$, **M**, provide an example of substantial interference [70]. The Fourier transform of these data are shown in Fig. 11. There is a peak at $R + \alpha = 2.6$ Å, which can plausibly be attributed to Mn···Mn XAFS at ca. 3.0 Å. However, if the data are modeled using only the first shell and a Mn···Mn shell, the apparent Mn···Mn distance refines to 3.1 Å, in contrast with the crystallo-graphic value of 3.3 Å. The correct Mn···Mn distance is only obtained when an additional Mn···(C/N) shell, representing outer shell scattering from the pyrazole rings, is included. This behavior is reminiscent of that seen for some of the Fe models. An important difference between **M** and the other Mn models, where Mn···(C/N) interference was not important, is that **M** has a relatively well ordered Mn···(C/N) shell at ca. 3 Å due to the high symmetry of the tris(pyrazolyl)borate ligand.

5.2. Protein studies

5.2.1. Manganese catalase

The dinuclear Mn site in Mn catalase can be prepared in a reduced, Mn(II)/Mn(II), form, an oxidized, Mn(III)/Mn(III), form, and a superoxidized, Mn(III)/Mn(IV) form [71]. The oxidized enzyme shows X-ray induced photo-
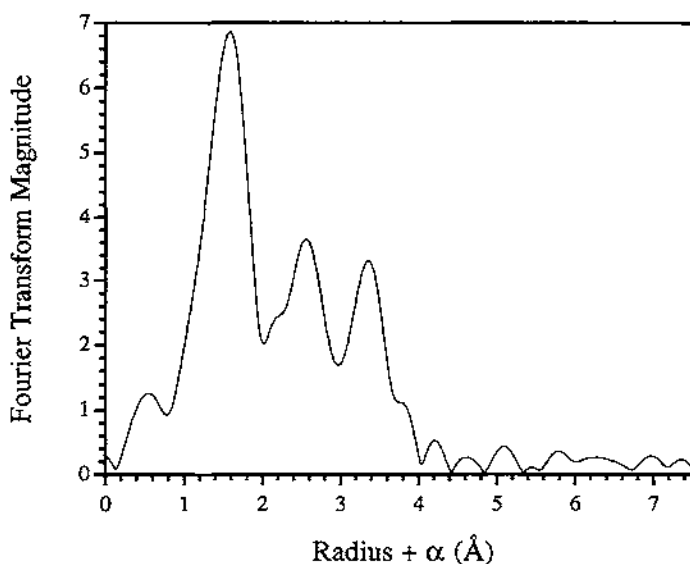

Fig. 11. Fourier transform of XAFS data for **M**, [Mn(II)(HB(3,5-iPr$_2$pz)$_3$]$_2$(OH)$_2$ over the k range = 1.5–11.5 Å^{-1}. The rigid pyrazole ring provides a strong Mn–N interaction at ≈ 3.1 Å that dominates the EXAFS and affects the refinement of the Mn···Mn contribution at 3.31 Å.

reduction; however, the other two derivatives have been studied by XAFS [72,73]. The superoxidized enzyme shows a well defined shell of 2 Mn–O_{oxo} bonds at 1.82 Å, a longer shell of 3–4 Mn–(O/N) at 2.1 Å, and a single Mn$\cdots$Mn interaction at about 2.68 Å. The observation that the Mn$\cdots$Mn distance was slightly less than 2.7 Å suggested [72] that there might be a μ-carboxylato bridge in addition to the two μ-oxo bridges, since Mn dimers that have only two oxo bridges generally have Mn$\cdots$Mn distances longer than 2.7 Å. As with the model compound studies, the short Mn$\cdots$Mn distance in the superoxidized catalase was readily detectable with no indications of interference from Mn$\cdots$C scattering. As noted previously, there is substantial interference between the μ-oxo XAFS and the Mn–(O/N) XAFS (see Figs. 9 and 10). This points to a well ordered shell of Mn–(O/N) scatterers with relatively long bond lengths. In model compounds, this is most consistent with nitrogen containing ligands and/or carboxylate ligands. Consistent with the former, there are additional peaks in the Fourier transform that can be attributed to Mn$\cdots$(C/N) scattering from imidazole ligands.

The XAFS for reduced Mn catalase is dramatically different from that for the superoxidized enzyme. The nearest-neighbor shell was fit with a single shell of low Z scatterers at 2.19 Å, with no evidence for a resolvable short Mn–O shell [72]. In this regard, Mn catalase resembles the reduced derivatives of the dinuclear Fe proteins, where the bridging ligand cannot be identified in the first shell XAFS. This could be due either to protonation of the Mn–O_{oxo} bridge(s) or to complete loss of the bridging oxo groups. The outer shell data for the reduced enzyme were modeled by Mn$\cdots$(C/N) interactions at 3.16 and 4.42 Å. Although it was possible to include an additional Mn$\cdots$Mn shell at distances between 3 and 4 Å, inclusion of this shell did not give a significant improvement in the quality of the fit. This indicates either that there is no significant contribution of a Mn$\cdots$Mn interaction to the XAFS or that, for data of the present resolution, it is not possible to reliably resolve Mn$\cdots$Mn from Mn$\cdots$(C/N) scattering. No refined crystal structures are available for Mn catalase to test the XAFS results. A low-resolution structure of the as-isolated, presumably oxidized, enzyme has been reported. This shows two maxima in electron density which can be assigned to the Mn atoms [74]. At this resolution, the apparent Mn$\cdots$Mn distance is 3.6 Å. If the actual Mn distance is this long, it is likely that the Mn$\cdots$Mn scattering would be very weak. It is thus not necessarily surprising that no Mn$\cdots$Mn XAFS signal could be resolved.

5.2.2. The oxygen evolving complex

There have been numerous XAFS studies of the manganese cluster that catalyzes the photosynthetic oxidation of water to molecular oxygen [75]. From the very earliest studies [61], the presence of a Mn$\cdots$Mn interaction at ca. 2.7 Å has been apparent. More recent work [76–78] has shown that there is also a Mn$\cdots$Metal interaction at ca. 3.3 Å. It now appears that the 3.3 Å interaction was not seen in the original studies because these measurements were made at 200 K. The more recent measurements have all been made at approximately 10 K. At this temperature, the outer shell peak is clearly detectable above the noise level. This is reminiscent of the early studies of hemerythrin, where the correct Fe$\cdots$Fe distance was not seen in

room temperature measurements. In contrast with hemerythrin, however, the OEC appears to lack the strong outer shell M···C interactions which led to erroneous assignments of M···M scattering at about 3.5 Å in the early hemerythrin work. One puzzling aspect of the outer shell XAFS for the OEC is a recent report [79] that the outer shell Mn···M distance is 3.7 Å rather than 3.3 Å. It is not yet clear what is responsible for this difference, since Mn···M vs. Mn···C interference does not appear to be important in the OEC.

The presence of a 2.7 Å Mn···Mn distance in the OEC suggests that di-μ-oxo bridged Mn dimers must be a minimal structural unit within the tetranuclear core. Based on this expectation, most of the XAFS studies of the OEC have fit the first shell data using a short Mn–O_{oxo} shell and a longer Mn–(O/N) shell [75,79]. However, in the most recent reports, the Mn–(O/N) shell is found to be highly disordered [69]. In order to obtain reasonable fits, the Debye–Waller factors and coordination numbers were constrained to the expected values. Under these conditions [69] the bond lengths refined to distances (1.81 and 1.90 Å) that are not resolvable by XAFS. A careful analysis of the degrees of freedom available in the first shell suggests that there probably is not an XAFS detectable Mn–O_{oxo} shell [67].

The absence of a resolved Mn–O_{oxo} interaction is reminiscent of the results for both Fe and Mn models, where in some cases there was no resolvable M–O_{oxo} shell, even though there were crystallographically characterized bridging oxo ligands. In the case of the OEC, the 2.7 Å Mn···Mn distance would seem to require the presence of oxo bridges, since, at this point, all of the model compounds with a Mn···Mn distance this short contain an Mn(μ-O)$_2$Mn core. The difference between the first shell XAFS for Mn catalase and for the OEC is striking (see Figs. 9 and 10). The presence of a readily resolvable oxo shell in the former was attributed to the catalase having relatively long Mn–(O/N) distances, similar to those seen in J and K. In contrast, the OEC may have a coordination sphere more similar to I, with short, ca. 1.95 Å Mn–O bonds, possibly from hydroxide, phenolate or alkoxide ligation, in addition to an Mn–(O/N) shell at a longer distance. It is clear that higher resolution (i.e., higher k) XAFS data will be necessary to define completely the OEC first coordination shell.

The OEC contains 4 Mn, in contrast with the 2 Fe or 2 Mn atoms present in all of the other proteins that have been discussed. This greatly complicates interpretation of the XAFS results, since there will inevitably be averaging of the contributions from the different Mn atoms. One promising approach to this problem is to measure XAFS spectra for oriented multilayers of the OEC. The observed linear X-ray dichroism can then be used to determine the relative orientation of different XAFS features and, in fortunate circumstances, to eliminate the averaging problem. Polarized measurements [76,80] suggest that the 3.3 Å Mn···M feature lies approximately parallel to the membrane normal, while the 2.7 Å features are more nearly perpendicular to the membrane normal. There are, however, substantial differences in the reported anisotropies of these features and additional work will be required to clarify the site structure. An exciting recent result is the finding that an oxidized state of the OEC shows increased disorder in the 2.7 Å feature. Based on the observed X-ray dichroism [80] this was attributed to a splitting of the Mn···Mn distances

into a 2.7 Å and a 2.8 Å component. It may thus be possible to use polarized measurements to resolve features that are not resolvable in isotropic XAFS.

6. Nickel XAFS

Urease contains a dinuclear Ni active site. On the basis of magnetism [81] and MCD measurements [82], it has been suggested that the two Ni(II) ions are antiferromagnetically coupled in the presence of the inhibitor 2-mercaptoethanol (2-ME). This implies that there should be an XAFS detectable Ni⋯Ni interaction, at least in the presence of 2-ME. Initial XAFS measurements [83] suggested that the Ni sites retain a distorted octahedral geometry in the presence of 2-ME, but did not show any clear evidence for Ni⋯Ni scattering. However, more recent measurements have identified the Ni⋯Ni distance as ca. 3.3 Å [84]. This is another illustration of the difficulty of identifying metal⋯metal interactions in proteins and, more importantly, this work suggests ways in which the combination of XAFS with other information can be used to extract structural information which would not be available from XAFS alone.

The initial data for 2-ME inhibited jack bean urease were interpreted in terms of 5 Ni–(O/N) ligands at 2.07 Å and a single Ni–S scatterer at 2.29 Å. In the more recent work, which included data for both the jack bean and the *K. aerogenes* urease, a more detailed first shell analysis gave 2 Ni–N$_{imidazole}$ scatterers at 2.05–2.06 Å, 2 Ni–(N/O) scatterers at 2.03–2.05 Å, and a single Ni–S scatterer at 2.23 Å [84]. Although there are small changes in the bond lengths for the two analyses, which were attributed to differences in the phase parameters used to model the XAFS, it is clear that both models describe the same average structure. The difference is that, in the more recent study, an attempt was made to distinguish between N$_{imidazole}$ first shell scattering and the scattering from other N/O containing ligands (the latter are most likely carboxylate ligands). On the surface, this would appear impossible, since the refined Ni–(N/O) distances differ by <0.02 Å, and are thus well below the resolution that is possible in XAFS (see Eq. 8).

In order to avoid this resolution limitation, Scott and co-workers fit the imidazole ligand as a rigid body [85]. In this approach, the ≈3 Å and ≈4 Å peaks in the Fourier transform are used to define the Ni–N$_1$ distance and the Ni–N$_1$–C$_2$ angle (see Fig. 1 for definitions). To the extent that the Ni lies in the plane of the imidazole and that the imidazole is the only group giving rise to the peaks at ≈3 Å and ≈4 Å, this approach should provide a good definition of the Ni–N$_1$ distance without the need for any first shell curve fitting. The Ni–N$_1$ distance can then be fixed and the remaining first shell scattering can be refined independent of interference from the N$_{imidazole}$ scattering.

It is a good assumption that the Ni lies in the plane of the imidazole. However, it is not necessarily clear that the ≈3 and ≈4 Å peaks can be associated uniquely with Ni-imidazole scattering. For urease + 2-ME, this approach appears to work, and indeed, it was the rigid-body definition of the imidazole that allowed the authors to identify the outer shell scattering from a Ni⋯Ni interaction at ca. 3.3 Å. If the

imidazole were not constrained to be a rigid body, there would not have been enough free parameters to justify the interpretation of this feature as Ni···Ni scattering. Even with this constraint, addition of the Ni···Ni scattering gives only a small (9%) improvement in the quality of the fit.

No crystallographic data are available at this point for urease. It remains to be seen how general this approach will prove to be. If the Ni···Ni interaction had been either shorter or longer than 3.3 Å, it would have interfered with the M···(C_2/C_5) or M···(N_3/C_4) peaks in the Fourier transform, thus potentially interfering with the analysis. Alternatively, the presence of bidentate carboxylates, which typically have M···C distances of 2.7–3 Å, could easily have complicated interpretation of the ≈ 3 Å peak as being due to Ni–(C_2/C_5) scattering. Nevertheless, this is a promising approach to the analysis of outer shell scattering and deserves further study. Greater use of multiple scattering calculations to improve the interpretation of outer shell data is likely to be useful in future studies of M···M interactions.

One final point worth noting is the importance of combining XAFS measurements with all of the other available data for a sample. In the case of urease + 2-ME, previous studies had pointed to the presence of a Ni···Ni interaction. With the availability of this information, Wang et al. could interpret the new peak as a 3.3 Å Ni···Ni interaction [84]. However, without the prior information that there should be a Ni···Ni interaction, it would have been difficult to prove its existence using XAFS alone.

7. Conclusions

It has been known for many years that XAFS can be used to obtain very accurate estimates of nearest neighbor bond lengths. Based on the results summarized here, it is clear that XAFS can also be used to obtain accurate M···M distances and to identify bridging ligands (e.g., bridging oxo groups). It is equally clear, however, that there are many cases where XAFS has failed to give reliable results. In attempting to understand the situations where XAFS succeeds and those where it fails, the following guidelines emerge.

7.1. High quality data are essential

Much of the early protein XAFS data (and some recent measurements) have suffered from very low signal/noise ratios and from very limited k ranges. A lower limit for k_{max} should be 12–13 Å^{-1}, and, wherever possible, the data should extend to higher k. Since the XAFS signal falls off approximately as $1/k^3$, plots of $\chi(k)\cdot k^3$ provide a convenient way to judge the size of the XAFS signal relative to the noise.

7.2. Accurate descriptions of all of the relevant scatterers are necessary

This includes M···C in addition to M···M XAFS. From a theoretical perspective, this problem now appears to be solved. The current generation of theoretical calcula-

tions give an excellent description of single scattering XAFS, at least above 1.5 Å^{-1}, and a reasonable description of multiple-scattering. This is illustrated by the ability of theoretical calculations to reproduce the XAFS spectra for model compounds.

This does not mean, however, that a complete description of the relevant scatterers is necessarily possible. If a metal site is completely uncharacterized, it may not be possible to determine the origin of an outer shell peak. In particular, unique discrimination between M···M and M···C scattering is often impossible using XAFS alone. This is essentially the situation described by Scott and Eidsness [7]. However, recent results suggest that the difficulties are not as severe as once thought. There are several examples in which XAFS has been used to predict accurate M···M distances in advance of crystallographic characterization. For a particular protein, it is always possible that M···M XAFS may not be detectable. This appears to be particularly likely for dinuclear sites having only hydroxo or aquo bridges. However, when M···M XAFS is detectable, it is usually possible to obtain an accurate M···M distance providing the M···C contributions can be described adequately.

7.3. Careful attention must be paid to the number of variable parameters

XAFS spectra contain only a limited amount of structural information. If the structure is known, for example in the case of a model compound, it may be possible to reproduce the observed spectra using all of the shells of scatterers. However, there is seldom sufficient information to permit reliable refinement of all of the possible structural parameters and attempts to do so in unknown systems can result in erroneous structural conclusions. This means that it is not always possible to detect bridging oxo ligands, even when they are known to be present, or that M···C XAFS may sometimes obscure M···M XAFS. As with other structural methods, the more that is known about a system, the easier it will be to obtain reliable structural information using XAFS.

A careful examination of the literature shows that, to a greater or lesser extent, most XAFS papers fail to provide sufficient information to permit readers to determine whether the above criteria have been met. The most serious problems are failures to describe the number of variable parameters, the Fourier filter range, and/or the statistics that have been used to decide on the significance of additional shells. There continue to be many papers in which the number of variables that are refined exceeds the amount of information that is present in the XAFS spectrum. Guidelines designed to improve this situation have recently been published and should, over time, improve the consistency of the XAFS literature [24].

8. Future prospects

When the conditions above are met, XAFS can provide unique, highly accurate structural information, including the identification and characterization of M···M interactions in dinuclear proteins. In general, XAFS analyses of M···M interactions seem to suffer from multiple-minima problems. However, if the appropriate minimum

can be defined from some other technique, then the model studies suggest that XAFS can provide extremely accurate distances.

Unfortunately, as a stand-alone technique, XAFS continues to be very limited in its ability to define uniquely M···M interactions. Several new developments, many centered on the new third-generation synchrotron sources, offer hope that the number of cases in which XAFS fails to provide unique information should decline in the future.

8.1. Data quality should improve

Protein XAFS spectra are typically measured as fluorescence excitation spectra [86]. The development of energy resolving solid state detectors has resulted in dramatically improved XAFS data quality for dilute samples by improving the discrimination between signal (e.g., Kα fluorescence) and noise (elastic and Compton scatter) [87]. However, substantial additional advances are still possible. These include improved detector speed (most current protein XAFS measurements are limited by the maximum count rate of the X-ray fluorescence detector [88]) and increased photon flux (depending on the energy, the new third-generation synchrotron sources will provide 1–2 orders of magnitude increase in flux). These, combined with improvements in beam stability, could improve the signal/noise ratio of XAFS spectra by 1–2 orders of magnitude, making it possible to extend protein XAFS data to much higher k ($k_{max} = 17$ Å^{-1} or higher). An extended k range would permit dramatically enhanced first shell resolution, as shown for some of the dinuclear Fe model compounds. It is important to note, however, that an extended data range will not, by itself, provide much improvement in Mn protein XAFS, since Mn XAFS data are typically limited by the presence of the Fe edge at ca. 12.2 Å^{-1} (due to the ubiquitous presence of Fe in biological samples). Similarly, the Zn edge typically limits biological Cu XAFS to $k \leqslant 13$ Å^{-1}. It may be possible to overcome even these limitations through the development of new energy resolving detectors with sufficient resolution to reject, for example, the Fe Kα photons that interfere with measurement of Mn XAFS spectra. If this proves possible, the resulting increase in k range should provide the resolution necessary to solve structural problems that at present remain ambiguous.

8.2. Polarized measurements can be used to increase the information content of an XAFS spectrum

The initial attraction of XAFS for studies of proteins was the fact that it could be used to provide structural information for samples that lacked long range order. However, if it is possible to orient a sample, the information that can be obtained from XAFS is greatly increased [89], as discussed above for the OEC [80]. With oriented samples, it is possible to measure XAFS spectra in two (or more) directions. This provides improved resolution, thus opening the possibility of resolving, from their orientation dependence, two scatterers that cannot be resolved in isotropic

XAFS. Alternatively, orientation dependence can eliminate the interference between, for example, M⋯C and M⋯M XAFS.

Samples may be oriented in three dimensions, that is, in crystals [90–92]. In this case, XAFS typically provides more accurate structural information for the metal site than can be obtained from a protein crystal structure. Alternatively, samples can be oriented in two dimensions, either by drying membrane bound proteins [93–95], or by preparing self-assembled monolayers of proteins [96]. In this case, XAFS can provide orientation information, i.e., the M⋯M direction, that is not available from any other method. Relatively little use has been made of polarized measurements to date. The new synchrotron sources will provide much brighter X-ray beams (i.e., more photons per mm^2) and will thus permit much greater use of polarized measurements.

8.3. Magnetic XAFS may permit reliable identification of M⋯M scattering

One of the most exciting recent developments in XAFS has been the recognition that X-ray magnetic circular dichroism (XMCD) studies are possible [97]. Most of this work has focused on using XMCD to study the magnetic properties of ferromagnetic materials, although there have also been some applications to proteins [98]. In the context of dinuclear metalloproteins, the most relevant experiment is one in which magnetic XAFS was used to isolate M⋯M' signals (M' has S ≠ 0) from all other scattering contributions [99]. The physical basis of this effect is the fact that absorption of circularly polarized X-rays results in creation of spin polarized photoelectrons. The spin state of the photoelectron has no effect on the XAFS unless the scatterer has a net spin. However, if the spin of the scatterer is oriented with respect to the photoelectron, there will be small differences in the XAFS spectra that are observed using left and right circularly polarized X-rays. This potentially means that spin polarized XAFS can be developed as a method for uniquely identifying M⋯M XAFS signals in paramagnetic proteins. The M⋯M signals will contribute to the circular dichroism, while the interfering M⋯C signals should be largely absent. This effect has been observed for solid state materials [99]. A great deal of work remains to be done on the theoretical interpretation of magnetic XAFS and on the development of facilities that can be used to measure magnetic XAFS for dilute samples. This technique offers the possibility, however, of uniquely isolating M⋯M XAFS from all of the interfering components. New beam lines are now being built to produce high flux, circularly polarized X-ray beams [100]. These should greatly improve the feasibility of X-ray MCD measurements for dilute samples.

Acknowledgments

References

[1] In various parts of the literature, the acronyms EXAFS (extended X-ray absorption fine structure), XANES (X-ray absorption near edge structure) and occasionally NEXAFS (near edge X-ray absorption fine structure) are used to refer to various parts of the X-ray absorption spectrum. With the development of improved theoretical models that can describe both the EXAFS and the XANES region, the acronym XAFS (X-ray absorption fine structure) has gained favor. This is the acronym that we will use.

[2] R.A. Scott, Methods Enzymol., 117 (1985) 414.

[3] B.K. Teo, EXAFS: Basic Principles and Data Analysis, Springer-Verlag, New York, 1986.

[4] S.P. Cramer, Chem. Anal., 92 (1988) 257.

[5] C.D. Garner, Adv. Inorg. Chem., 36 (1991) 303.

[6] C.D. Garner, in C.R.A. Catlow and G.N. Greaves (eds.), Applications of Synchrotron Radiation, Blackie, Glasgow, 1990, p. 268.

[7] R.A. Scott and M.K. Eidsness, Comm. Inorg. Chem., 7 (1988) 235.

[8] P.A. Lee, B.K. Teo and A.L. Simons, J. Am. Chem. Soc., 99 (1977) 3856.

[9] B.K. Teo and P.A. Lee, J. Am. Chem. Soc., 101 (1979) 2815.

[10] B.K. Teo, M.R. Antonio and B.A. Averill, J. Am. Chem. Soc., 105 (1983) 3751.

[11] A.G. McKale, G.S. Knapp and S.K. Chan, Phys. Rev. B., 33 (1986) 841.

[12] A.G. McKale, B.W. Veal, A.P. Paulikas, S.K. Chan and G.S. Knapp, J. Am. Chem. Soc., 110 (1988) 3763.

[13] A.G. McKale, G.S. Knapp, B.W. Veal, A.P. Paulikas and S.K. Chan, Physica B, 158 (1989) 355.

[14] M. Vaarkamp, I. Dring, R.J. Oldman, E.A. Stern and D.C. Koningsberger, Phys. Rev. B, 50 (1994) 7872.

[15] J.J. Rehr, R.C. Albers, C.R. Natoli and E.A. Stern, J. Phys., Colloq., 1 (1986) C8/31.

[16] J.J. Rehr, d.L.J. Mustre, S.I. Zabinsky and R.C. Albers, J. Am. Chem. Soc., 113 (1991) 5135.

[17] J.J. Rehr, R.C. Albers and d.L.J. Mustre, Physica B, 158 (1989) 417.

[18] S.J. Gurman, N. Binsted and I.J. Ross, Physica C, 17 (1984) 143.

[19] N. Binsted, R.W. Strange and S.S. Hasnain, Biochemistry, 31 (1992) 12117.

[20] R.W. Strange, N.J. Blackburn, P.F. Knowles and S.S. Hasnain, J. Am. Chem. Soc., 109 (1987) 7157.

[21] B.K. Teo, J. Am. Chem. Soc., 103 (1981) 3990.

[22] J.J. Rehr, R.C. Albers and S.I. Zabinsky, Phys. Rev. Lett., 69 (1992) 3397.

[23] T.E. Westre, A. DiCicco, A. Filliponi, C.R. Natoli, B. Hedman, E.I. Solomon and K.O. Hodgson, J. Am. Chem. Soc., 117 (1995) 1566.

[24] G. Bunker, S. Hasnain and D. Sayers, in S.S. Hasnain (ed.), X-ray Absorption Fine Structure, Ellis Horwood, New York, 1991, p. 751.

[25] E.A. Stern, Phys. Rev. B, 48 (1993) 9825.

[26] E.A. Stern, Jpn. J. Appl. Phys., 1 (1993) 851.

[27] (a) P.A. Lee, P.H. Citrin, P. Eisenberger and B.M. Kincaid, Rev. Mod. Phys., 53 (1981) 769. (b) G. Bunker, Instrum. Methods Phys. Res., 207 (1983) 437.

[28] N.J. Blackburn, M.E. Barr and W.H. Woodruff, J. van der Ooost and S. de Vries, Biochemistry, 33 (1994) 10401.

[29] D.M. Dooley, M.A. McGuirl, A.C. Rosenzweig, J.A. Landin, R.A. Scott, W.G. Zumft, F. Devlin and P.J. Stephens, Inorg. Chem., 30 (1991) 3006.

[30] G.N. George, S.P. Cramer, T.G. Frey and R.C. Prince, Biochim. Biophys. Acta, 1142 (1993) 240.

[31] R.A. Scott, W.G. Zumft, C.L. Coyle and D.M. Dooley, Proc. Natl. Acad. Sci. USA, 86 (1989) 4082.

[32] C.K. SooHoo, C.K. Hollocher, A.F. Kolodziej, W.H. Orme-Johnson and G.J. Bunker, Biol. Chem., 266 (1991) 2210.

[33] W.H. Armstrong, A. Spool, G.C. Papaefthymiou, R.B. Frankel and S.J. Lippard, J. Am. Chem. Soc., 106 (1984) 3653.

[34] W.H. Armstrong and S.J. Lippard, J. Am. Chem. Soc., 106 (1984) 4632.

[35] S.M. Kauzlarich, B.K. Teo, T. Zirino, S. Burman, J.C. Davis and B.A. Averill, Inorg. Chem., 25 (1986) 2781.

[36] B. Hedman, M.S. Co, W.H. Armstrong, K.O. Hodgson and S.J. Lippard, Inorg. Chem., 25 (1986) 3708.

[37] R.C. Scarrow, M.J. Maroney, S.M. Palmer, L. Que, Jr., S.P. Salowe and J. Stubbe, J. Am. Chem. Soc., 108 (1986) 6832.

[38] A.E. True, R.C. Scarrow, C.R. Randall, R.C. Holz and L.J. Que, J. Am. Chem. Soc., 115 (1993) 4246.

[39] A. Ericson, B. Hedman, K.O. Hodgson, J. Green, H. Dalton, J.G. Bentsen, R.H. Beer and S.J. Lippard, J. Am. Chem. Soc., 110 (1988) 2330.

[40] B. Hedman, M.S. Co, W.H. Armstrong, K.O. Hodgson and S.J. Lippard, Inorg. Chem., 25 (1986) 3708.

[41] Y. Zang, G. Pan, L. Que, Jr., B.G. Fox, E. Münck, J. Am. Chem. Soc., 116 (1994) 3653.

[42] W.T. Elam, E.A. Stern, J.D. McCallum and L.J. Sanders, J. Am. Chem. Soc., 104 (1982) 6369.

[43] W.A. Hendrickson, M.S. Co, J.L. Smith, K.O. Hodgson and G.L. Klippenstein, Proc. Natl. Acad. Sci. USA, 79 (1982) 6255.

[44] M.A. Holmes and R.E. Stenkamp, J. Mol. Biol., 220 (1991) 723.

[45] W.A. Hendrickson, in J. Lamy (ed.), Invertebrate Oxygen-Binding Proteins: Structure, Active Site and Function, Marcel-Dekker, New York, 1981, p. 503.

[46] R.E. Stenkamp, L.C. Sieker and L.H. Jensen, Acta Crystallogr. B, 39 (1983) 697.

[47] M.S. Co, W.A. Hendrickson, K.O. Hodgson and S. Doniach, J. Am. Chem. Soc., 105 (1983) 1144.

[48] R.C. Scarrow, M.J. Maroney, S.M. Palmer, L. Que, Jr., A.L. Roe, S.P. Salowe and J. Stubbe, J. Am. Chem. Soc., 109 (1987) 7857.

[49] K. Zhang, E.A. Stern, F. Ellis, L.J. Sanders and A.K. Shiemke, Biochemistry, 27 (1988) 7470.

[50] W.T. Elam, E.A. Stern, J.D. McCallum and L.J. Sanders, J. Am. Chem. Soc., 105 (1983) 1919.

[51] M.A. Holmes, T.I. Le, S. Turley, L.C. Sieker and R.E. Stenkamp, J. Mol. Biol., 218 (1991) 583.

[52] R.E. Stenkamp, L.C. Sieker and L.H. Jensen, Acta. Crystallogr. B, 38 (1982) 784.

[53] G. Bunker, L. Petersson, B.M. Sjoeberg, M. Sahlin, M. Chance, B. Chance and A. Ehrenberg, Biochemistry, 26 (1987) 4708.

[54] P. Nordlund and H.J. Eklund, Mol. Biol., 232 (1993) 123.

[55] R.C. Prince, G.N. George, J.C. Savas, S.P. Cramer and R.N. Patel, Biochim. Biophys. Acta, 952 (1988) 220.

[56] DeWitt, J.B. Hedman, A. Ericson, K.O. Hodgson, J. Bentsen, R. Beer, S.J. Lippard, J. Green and H. Dalton, Physica B, 158 (1989).

[57] J.G. DeWitt, J.G. Bentsen, A.C. Rosenzweig, B. Hedman, J. Green, S. Pilkington, G.C. Papaefthymiou, H. Dalton, K.O. Hodgson and S.J. Lippard, J. Am. Chem. Soc., 113 (1991) 9219.

[58] A.C. Rosenzweig, C.A. Frederick, S.J. Lippard and P. Nordlund, Nature, 366 (1993) 537.

[59] J.E. Sarneski, M. Didiuk, H.H. Thorp, R.H. Crabtree, G.W. Brudvig, J.W. Faller and G.K. Schulte, Inorg. Chem., 30 (1991) 2833.

[60] S. Drücke, K. Wieghardt, B. Nuber, J. Weiss, H.-P. Fleischhauer, S. Gehring and W. Haase, J. Am. Chem. Soc., 111 (1989) 8622.

[61] J.A. Kirby, A.S. Robertson, J.P. Smith, A.C. Thompson, S.R. Cooper and M.P. Klein, J. Am. Chem. Soc., 103 (1981) 5529.

[62] V. Pecoraro, D. Kessissoglou, X. Li, M.S. Lah, S. Saadeh, C. Bender, J. Bonadies and E. Larson, in M. Baltscheffsky (ed.), Current Research in Photosynthesis, Kluwer, Dordrecht, 1990, Vol. I, p. 709.

[63] E.J. Larson and V.L. Pecoraro, in V. Pecoraro (ed.), Manganese Redox Enzymes, VCH, 1992.

[64] E. Larson, M.S. Lah, X. Li, J.A. Bonadies and V.L. Pecoraro, Inorg. Chem., 31 (1992) 373.

[65] E.J. Larson, P.J. Riggs, J.E. Penner-Hahn and V.L. Pecoraro, J. Chem. Soc., Chem. Commun., (1992) 102.

[66] M.J. Baldwin, T.L. Stemmler, P.J. Riggs-Gelasco, M.L. Kirk, J.E. Penner-Hahn and V.L. Pecoraro, J. Am. Chem. Soc., 116 (1994) 11349.

[67] P.J. Riggs-Gelasco, R. Mei, C.F. Yocum and J.E. Penner-Hahn, submitted, J. Am. Chem. Soc.
[68] C.F. Yocum, in V.L. Pecoraro (ed.), Manganese Redox Enzymes VCH, New York, 1992, p. 71.
[69] V.J. DeRose, I. Mukerji, M.J. Latimer, V.K. Yachandra, K. Sauer and M.P. Klein, J. Am. Chem. Soc., 116 (1994) 5239.
[70] P.J. Riggs-Gelasco, T.L. Stemmler, A.K. Gelasco, N. Kitajima, V.L. Pecoraro and J.E. Penner-Hahn, manuscript in preparation.
[71] J.E. Penner-Hahn, in V.L. Pecoraro (ed.), Manganese Redox Enzymes VCH, New York, 1992, p. 29.
[72] G.S. Waldo, S. Yu and J.E. Penner-Hahn, J. Am. Chem. Soc., 114 (1992) 2.
[73] T.L. Stemmler, D. Randall, B. Sturgeon, R.D. Britt and J.E. Penner-Hahn, manuscript in preparation.
[74] B.K. Vainshtein, A.W.R. Melik, V.V. Barynin, A.A. Vagin and A.I. Grebenko, J. Biosci., 8 (1985) 471.
[75] K. Sauer, V.K. Yachandra, R.D. Britt and M.P. Klein, in V.L. Pecoraro (ed.), Manganese Redox Enzymes VCH, New York, 1992.
[76] G.N. George, R.C. Prince and S.P. Cramer, Science, 243 (1989) 789.
[77] J.E. Penner-Hahn, R.M. Fronko, V.L. Pecoraro, C.F. Yocum, S.D. Betts and N.R. Bowlby, J. Am. Chem. Soc., 112 (1990) 2549.
[78] V.K. Yachandra, V.J. DeRose, M.J. Latimer, I. Mukerji, K. Sauer and M.P. Klein, Science, 260 (1993) 675.
[79] D.J. MacLachlan, B.J. Hallahan, S.V. Ruffle, J.H.A. Nugent, M.C.W. Evans, R.W. Strange and S.S. Hasnain, Biochem. J., 285 (1992) 569.
[80] I. Mukerji, J.C. Andrews, V.J. DeRose, M.J. Latimer, V.K. Yachandra, K. Sauer and M.P. Klein, Biochemistry, 33 (1994) 9712.
[81] P.A. Clark and D.E. Wilcox, Inorg. Chem., 28 (1989) 1326.
[82] M.G. Finnegan, A.T. Kowal, M.T. Werth, P.A. Clark, D.E. Wilcox and M.K. Johnson, J. Am. Chem. Soc., 113 (1991) 4030.
[83] P.A. Clark, D.E. Wilcox and R.A. Scott, Inorg. Chem., 29 (1990) 579.
[84] S. Wang, M.H. Lee, R.P. Hausinger, P.A. Clark, D.E. Wilcox and R.A. Scott, Inorg. Chem., 33 (1994) 1589.
[85] R.A. Scott, S. Wang, M.K. Eidsness, A. Kriauciunas, C.A. Frolik and V.J. Chen, Biochemistry, 31 (1992) 4596.
[86] J. Jaklevic, J.A. Kirby, M.P. Klein, A.S. Robertson, G.S. Brown and P. Eisenberger, Solid State Commun., 23 (1977) 679.
[87] S.P. Cramer, O. Tench, M. Yocum and G.N. George, Nucl. Instrum. Methods Phys. Res. A, 266 (1988) 586.
[88] J.L. Smith and K.D. Watenpaugh (eds.), Structural Biology and Synchrotron Radiation: Assessment of Resources and Needs, BioSync, West Lafayette, 1991.
[89] J.E. Hahn and K.O. Hodgson, Acs Symp. Ser., 211 (1983) 431.
[90] R.A. Scott, J.E. Hahn, S. Doniach, H.C. Freeman and K.O. Hodgson, J. Am. Chem. Soc., 104 (1982) 5364.
[91] S.E. Shadle, J.E. Penner-Hahn, H.J. Schugar, B. Hedman, K.O. Hodgson and E.I. Solomon, J. Am. Chem. Soc., 115 (1993) 767.
[92] J. Chen, J. Christiansen, N. Campobasso, J.T. Bolin, R.C. Tittsworth, B.J. Hales, J.J. Rehr and S.P. Cramer, Angew. Chem., 105 (1993) 1661.
[93] G.N. George, S.P. Cramer, T.G. Frey and R.C. Prince, Biochim. Biophys. Acta, 1142 (1993) 240.
[94] G.N. George, R.C. Prince, T.G. Frey and S.P. Cramer, Physica B, 158 (1989) 81.
[95] G.N. George, S.P. Cramer, T.G. Frey and R.C. Prince, in C.H. Kim (ed.), Advances in Membrane Biochemistry and Bioenergetics, Plenum, New York, 1987, p. 429.
[96] S.M. Amador, J.M. Pachence, R. Fischetti, J.P. McCauley, A.B. Smith and J.K. Blasie, Langmuir, 9 (1993) 812.
[97] Schutz, G.W. Wagner, W. Wilhelm, P. Kienle, R. Zeller, R. Frahm and G. Matterlik, Phys. Rev. Lett., 58 (1987) 737.
[98] J. van Elp, S.J. George, J. Chen, G. Peng, C.T. Chen, L.H. Tjeng, G. Meigs, H.J. Lin, Z.H. Zhou, M.W.W. Adams, B.G. Searle and S.P. Cramer, Proc. Natl. Acad. Sci. USA, 90 (1993) 9664.
[99] G. Schutz, R. Frahm, P. Mautner, R. Wienke, W. Wagner, W. Wilhelm and P. Kienle, Phys. Rev. Lett., 62 (1989) 2620.
[100] A. Fontaine, Jpn. J. Appl. Phys., 32-2 (1993) 856.